Katrine Meinseth

Fatigue Design of Cables for Energy Transport

Master's thesis in Engineering Design and Materials
Supervisor: Filippo Berto
Co-supervisor: Antonio Alvaro

June 2020

Master's thesis

NTNU
Norwegian University of Science and Technology
Faculty of Engineering
Department of Mechanical and Industrial Engineering

NTNU

Norwegian University of
Science and Technology

Katrine Meinseth

Fatigue Design of Cables for Energy Transport

Master's thesis in Engineering Design and Materials
Supervisor: Filippo Berto
Co-supervisor: Antonio Alvaro
June 2020

Norwegian University of Science and Technology
Faculty of Engineering
Department of Mechanical and Industrial Engineering

NTNU
Norwegian University of
Science and Technology

Abstract

Underwater power cables are used to distribute power to offshore installations. The power cables consist of internal conductors that are protected by different layers of material. A lead sheathing works a protective layer against seawater penetration. During extrusion of the lead sheathings, it sometimes occurs small impurities or irregularities in the material. The power cables are subject to cyclic loading, and they must withstand the loading conditions. The investigation of the fatigue life and material response of the Pb-Sb-Sn alloy used in the lead sheathings is highly important, especially looking at the impact of irregularities. The procedure is complicated due to the materials' high ductility and low melting temperature, leading to time-dependent deformation as creep at room temperature.

The purpose of this thesis is to investigate how irregularities impact the fatigue life of lead sheathings. Results from experimental testing have been used to create a material model that replicates the material response to cyclic loading using Isight. The power law creep model has been applied, given a sufficient fit. Finite element models with and without irregularities have been made in Abaqus to investigate the impact on fatigue life. Strain-life curves have been obtained from fatigue tests with strain rates of $1\text{E-}2s^{-1}$ and $1\text{E-}3s^{-1}$, for both the highest equivalent Von Mises strain and the nominal strain for models with and with irregularities.

The thesis provides a substantial literature and theory review, followed by an investigation of fatigue life. Results indicate a shortened fatigue life due to the presence of irregularities. Reduction in life was, on average 70% for tests with a strain rate of $1\text{E-}2s^{-1}$ and 30% with a strain rate of $1\text{E-}3s^{-1}$. In future work, it is recommended to obtain accurate measurements of the irregularities to use in finite element modeling and testing. There should be conducted more tests with the same loading modes for specimens with and without irregularities.

Sammendrag

Under vann brukes strømkabler til å distribuere strøm til offshoreinstallasjoner. Strømkablene består av innvendige strømledere som er beskyttet av flere lag med materiale. Ekstruderte blyhylser fungerer som et beskyttende lag mot inntrenging av sjøvann. Under ekstrudering av disse hylsene av bly kan det forekomme små ujevnheter i materialet. Strømkablene blir utsatt for syklisk belastning, og det er avgjørende at de tåler belastningen kablene blir utsatt for. I det beskyttende laget er det en Pb-Sb-Sn-legering som brukes. Det er av stor interesse å beregne utmattingslevetiden til dette beskyttende laget, og da spesielt med tanke på effekten av ujevnhetene. Dette er komplisert å undersøke på grunn av materialets høye duktilitet og lave smeltetemperatur, noe som fører til tidsavhengig deformasjon allerede ved romtemperatur.

Hensikten med denne oppgaven er å undersøke hvordan ujevnheter påvirker utmattelseslevetiden til blyhylser. Resultater fra fysiske tester er blitt brukt til å lage en materialmodell som gjenskaper materialresponsen til syklisk belastning ved bruk av Isight. "Power law"-modellen er brukt, noe som har gitt tilfredsstillende resultater. Det er laget FEM i Abaqus, både med og uten ujevnheter, for å teste hvordan dette påvirker utmattingslevetiden. Videre har det blitt laget kurver med tøyning mot levetid for tester utført med en tøyningshastighet på 1E-2s^{-1} og 1E-3s^{-1}. Dette har blitt gjort med det som tilsvarer den høyeste Von Mises-tøyningen og den nominelle tøyningen, for modeller med og uten ujevnheter.

Oppgaven består av en solid litteratur- og teorigjennomgang, etterfulgt av utredning av utmattingslevetiden for blyhylsene. Resultatene indikerer at levetiden er noe forkortet på grunn av tilstedeværelsen av ujevnheter, hvor den gjennomsnittlige reduksjonen er 70 % for testene med en tøyningshastighet på 1E-2s^{-1} og 30 % for testene med en tøyningshastighet på 1E-3s^{-1}. I fremtidig arbeid er det anbefalt å bruke mer nøyaktige målinger av ujevnhetene som forekommer i blyhylsene, for bruk i FEM og testing. Det bør utføres flere tester der like lasttilfeller benyttes, både med og uten ujevnheter.
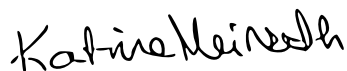
Preface

This master thesis is written as the final specialization at the Faculty of Engineering for the degree of Master of Science in Mechanical Engineering at the Norwegian University of Science and Technology (NTNU). The thesis is written as a collaboration with SINTEF and as a part of a research project between SINTEF and NEXANS. The results obtained in this thesis will contribute to the NASCAR project.

The master thesis builds on the specialization project carried out in the fall semester before this master. The project investigated strain rate dependency of lead in sheathings, which is an essential factor in the studies in this thesis. The relevant theory and literature reviews are therefore implemented in this master thesis.

The thesis's primary focus is on how irregularities impact the fatigue life of lead sheathings in underwater power cables. The fundamentals of the research are based on finite element analysis in Abaqus and the results from physical testing by digital image correlation, where the fatigue life and the impact of irregularities have been studied. The results will be used for further research to optimize lead sheathings in the future.

Katrine Meinseth, Trondheim, June 2020

Table of Contents

List of Tables

List of Figures

Abbreviations and Symbols

DIC	=	Digital Image Correlation
FEA	=	Finite Element Analysis
FEM	=	Finite Element Method
XLPE	=	High Density Polyethylene
MI	=	Mass-Impregnated
σ	=	Stress
ϵ	=	Strain
$\dot{\epsilon}$	=	Strain rate
F	=	Force
t	=	Time
T	=	Temperature
T_m	=	Absolute melting temperature
Q_c	=	Activation energy for creep
Q_{sd}	=	Activation energy for self-diffusion
k_t	=	Elastic stress concentration factor
k_f	=	Fatigue notch factor
q	=	Notch sensitivity
E	=	Young's modulus
ν	=	Poisson's ratio
$\triangle\epsilon$	=	Strain range
n	=	Steady state stress exponent
N	=	Stress sensitivity exponent

Chapter 1

Introduction

1.1 Background

Subsea power cables are used for power delivery to offshore installations. The power cables are installed on the seabed and connected to production facilities through risers. As a result of this, the cables are subject to cyclic loading caused by waves and vessel movements. The power cables usually consist of copper or aluminum conductors and lead sheathings. An example of a subsea power cable can be seen in **Fig.1.1**. The lead sheathing is a protective layer against water penetration. Loads to the cables from waves, current, and installation movement may be difficult to estimate correctly as the subsea environment is dominated by various cyclic loads. Hence, it is difficult to estimate the effect on the cable as well.

If some part of the cable goes to fracture or gets ruined by fatigue, it can have fatal consequences and system failure. It is therefore of interest to get an understanding of how the cyclic loading influences the power cables and the components inside it. The lead sheathing is a complicated and vital component to investigate. Lead is a ductile material with a low melting temperature, high malleability, and it is strain rate dependent. These properties make it challenging to investigate creep- and fatigue behaviour. When the lead sheathings are extruded, there might be irregularities in the material, due to particles entering the metal lattice. The irregularities that can occur in the material might impact the fatigue life of the lead sheathings. Because failure may cause severe consequences, fatigue behaviour and notch impact of the material should be investigated further (Nexans, 2019; Hofgaard, 2018; Viespoli et al., 2019b).

1.2 Objective

This master thesis is a part of the NASCAR project in collaboration with SINTEF and Nexans. The main objective of the thesis is to implement a material model that is able to

Figure 1.1: An example of a subsea power cable from Nexans (Nexans, 2019).

describe both the monotonic and the cyclic behaviour of lead. The material model will be used to study the impact of geometrical irregularities in order to quantify their impact on both the local strain distribution and the global load conditions effects, such as out-of-plane bending effects, in a test environment. The results and the analysis of the finite element simulation will be used to provide a better understanding of the fatigue life of lead cable sheathing, particularly concerning the extent of the impact of the geometrical imperfection inherent to the production of the cables.

Thesis Outline

The rest of the thesis will be structured as follows:

- Chapter 1 presents a literature review on the topic.

- Chapter 2 contains a review of theory related to the topics in this thesis.

- Chapter 3 presents the material model calibration.

- Chapter 4 contains the set up and procedure for fatigue testing.

- Chapter 5 presents a discussion of the method and results from the previous chapters.

- Chapter 6 contains of two parts: the main conclusion summarizing the work and recommended further work on the topic

1.3 Literature Review

A literature review has been conducted to assess the current knowledge of the relevant topic. The literature review has revealed that the existing research on the behaviour of

lead sheathing used in subsea power cables is minimal. Multiple industries would benefit from a more in-depth investigation of the topic, as the power cables are utilized both in the oil and gas industry and in the electrical power transmission industry. Due to the small amount of knowledge about the topic, the lead sheathings produced today are conservative to ensure a long enough service life. This research can, therefore, help minimize the thickness of the sheathings, resulting in lower costs in the future.

Multiple factors influence the fatigue life of the lead sheathings. This research concentrates on looking into the creep- and fatigue behaviour of lead and how geometrical irregularities have an impact on fatigue life. The knowledge obtained will help implement a material model that describes the monotonic and cyclic behaviour of lead, including the extent of the impact of geometrical irregularities.

The article "Room temperature creep mechanisms of a Pb-Sn-Sb lead alloy" by Viespoli et al. (2019a) has been reviewed. In the article, the authors investigate how the given alloy behaves during a series of tensile tests. The tests in the article give insight into what deformation mechanisms might be active during the life of the lead sheathings used in power lines. Viespoli et al. (2019a) utilized the Anand creep model in the article, which is a model that is able to recreate the creep in the two first stages. Both temperature- and strain hardening effects are included in the model. To calibrate the model, tensile tests at nominal strain rates of $1E\text{-}7s^{-1}$, $1E\text{-}5s^{-1}$ and $1E\text{-}3s^{-1}$, and a relaxation test from 10 MPa were performed. The results from these tests were connected through an Isight loop (Dassault Systems, 2017), to obtain a good agreement between the experimental results and the numerical model. Steady state creep behaviour was looked into, and a tensile test with several steps at different stress levels was conducted to obtain an exponent correlating stress and strain rate for steady state creep. This exponent was found to be between 3 and 12 MPa. The article (Viespoli et al., 2019a) concludes with:

- The results indicate that diffusional creep mechanisms are active in low stress ranges, from 3 to 5 MPa.

- Dislocation creep mechanism is the primary mechanism for the higher stress ranges.

- More research and further testing are necessary for different average grain size in low stress ranges, to resolve what type of diffusional creep is predominant.

Another relevant article that has been reviewed is "Tensile characterization of a lead alloy: creep induced strain rate sensitivity" by Viespoli et al. (2019c). In this article, the authors investigate the tensile properties of the lead alloy utilized in cable sheathings. The strain rate sensitivity, in particular, is being investigated due to creep being already present at room temperature. The material utilized for testing was extruded into a pipe, with three different thicknesses: 1.1, 1.8, and 3.3 mm. The metallurgical investigation uncovered that the average grain size in the 1.1mm and 1.8mm thick specimens were approximately the same, while the average grain size for the 3.3mm thick specimen was larger. The different average grain size have a considerable influence on creep behaviour and the material's mechanical response. The paper aims to provide a suitable material model of the alloy able to reproduce the material behaviour in a finite element analysis. There were performed

tensile tests with three different strain rates, $1E\text{-}7s^{-1}$, $1E\text{-}5s^{-1}$ and $1E\text{-}3s^{-1}$, for the three different specimen thicknesses. Both primary and secondary creep was present during the tests. The results indicate that the thickness and the strain rate are two major factors influencing the material's tensile response. The authors looked into both the power law creep model and the Anand creep model. The main conclusions of the article (Viespoli et al., 2019c) are:

- The power law creep model is desirable for its simplicity at the higher strain rates.

- The Anand creep model performed better for the lower strain rates.

- The power law creep model describes the primary creep region.

- The Anand creep model describes the primary and secondary creep regions.

- With thicker extrusions, the average grain size is bigger, resulting in improved resistance.

In the article "Small- and Full-Scale Fatigue Testing of Lead Cable Sheathing" by Johanson et al. (2019), the aim was to understand the transferability between scales and testing methods for lead sheathings. The authors conducted tests with two different loading modes on both small- and full-scale components: reverse bending and tension-compression. The full scale tests were conducted on Mass-Impregnated power cables (MI) and Cross-Linked High Density Polyethylene power phases (XLPE). An XLPE power cable often consists of three XPLE power phases stranded together. As fatigue-creep interaction is highly important, creep influence and strain rate sensitivity was of high interest. For small-scale testing, 44 reverse bending tests were conducted with 11 different test parameters and eight tension-compression tests with different strain ranges and constant strain rate. 27 XLPE power phases and 30 MI power cables were subjected to reverse bending. These tests led to the main conclusions by Johanson et al. (2019):

- The fatigue life of lead strongly depends on loading mode.

- For small-scale testing, results indicate significantly improved fatigue life compared to tension-compressing. When a power cable is subjected to bending, the lead sheathings experience mostly tension-compressing load. Due to this, it is not advisable to base fatigue life calculation of tubular lead sheathings solely from reverse bending of small-scale specimens.

- The fatigue life is greatly improved when tested in a MI power cable compared to small-scale testing. However, this is not the case with XLPE power phases. The results from the XLPE power phases do potentially overlap with the small-scale tests, but additional experiments are necessary.

- The results extracted from reverse bending tests fit relatively well with the results from the full scale testing of the MI power cables. Care should be taken when extrapolating the test results outside the test range due to the strain rate sensitivity not being based on tests reflecting the correct loading mode.

- Most of the fractures on full scale tests appear to initiate in surface discontinuities. The effect of the discontinuities is different for MI power cables and XPLE power phases. This could possibly indicate positive effects as a result of the negative effects of the discontinuities.

In the article "Strain controlled medium cycle fatigue of a notched Pb-Sn-Cd lead alloy" by Viespoli et al. (2019b), the authors investigate the impact of irregularities in lead sheathings. These irregularities may occur by particles entering the metal lattice during production. Specimens retrieved directly from the extruded sheathing, both with and without irregularities, have been fatigue tested. This was done to establish the effects irregularities have on the fatigue life and integrity of the sheathing. Notched and un-notched specimens were tested at the frequencies of 5 and 10 Hz for two strain ranges, 0.15%, and 0.28%. There were performed tensile tests to characterize the materials tensile properties. Two different batches of fatigue testing were completed, where the second one used digital image correlation. In the first batch, with the higher strain range and lowest frequency, the results indicated no influence of the presence of notches in terms of numbers of cycles to failure. For all the specimens, the failures started from the edge and propagated towards the middle through the notch for the notched specimens. For the tests at the lower strain range, at both frequencies, the notched specimens had a shorter fatigue life than the un-notched specimens. The cracks seemed to be more randomly positioned, not starting from the notch, but from the edges of the specimens, at the fillet radius, or the height of the notch. There was no significant correlation with the presence of the discontinuity. For the second batch, the notched specimens tested at 10 Hz showed cracks that were also originating from the notch, while the tests at 5 Hz showed no cracking at the notch. This could be a result of the material having a higher notch sensitivity at higher strain rates. The test results and investigation led to the following main conclusions by Viespoli et al. (2019b):

- The highly plastic behaviour of the tested alloy yields to a minimal notch sensitivity, with fatigue cracks starting from other locations than the notch with higher geometrical stress concentration factor.

- The small irregularities should try to be avoided but do not constitute a high threat to the structural integrity of the lead sheathings.

- The propagation of the fatigue cracks in a plastic material in fully reversed load is strongly influenced by mode II fracture propagation.

In the article "Experimental and numerical investigation of strain distribution of notched lead fatigue test specimen" by Johanson et al. (2018), the focus is on the test methodology related to the effect of stress concentration in strain-controlled structures. The lead sheathings in underwater cables often consist of multiple discontinuities, this results in intensified local stress and strain fields. Lead sheathings from power cables are investigated by the use of cyclic fatigue testing, Digital Image Correlation, and 3D Finite Element Analysis, where the focus is to investigate the strain distribution and fatigue failure of notched specimen extracted from cable sheathings. The test material was extracted from a power cable, and a notch was made by electro discharge machining on the convex surface of the specimen. Cyclic tension-compression fatigue testing directed towards reversed bending of a power cable was conducted to investigate the impact of discontinuity on fatigue life.

The tests were performed with a constant strain range target values of 0.28% and 0.15% and a frequency of 5 and 10 Hz. It was observed a decrease in the nominal amplitude for the notched specimens. Relaxation causes a strong strain rate dependency for lead alloys tested under displacement control. A series of tensile tests were conducted to identify the strain rate dependency and a suitable material model for the finite element modeling.

To investigate the stress distribution in the specimen during the fatigue testing in relation to the failure location and final fatigue life from the fatigue testing, finite element analysis have been utilized. The results from the experimental testing show that at the higher strain range (0.28%) the notch impact on fatigue life is practically none. For the test with the lower strain range (0.15%) and 5 Hz however, the fatigue life decreases by about 65% due to the presence of a notch. They also observed that by going from 5 to 10 Hz the impact of the notch seems to have decreased, while the fatigue life of the un-notched specimen drops by about 40%. At 0.15% and 10 Hz the notch impact seemed to be insignificant. Analysis done after the tests illustrated differences in the crack location, which indicate that the presence of a notch induces a variation in the stress/strain field strong enough to change the point of crack initiation, but the weakest point of the specimen seems to be the edge when it comes to crack initiation. The finite element analysis were performed to try to understand the impact of the notch on the failure dynamics and to eventually reproduce the behaviour of the alloy numerically. The FEM analysis results indicate that the notched specimen shows a higher strain at comparable equivalent boundary displacement. According to the authors, this justifies the final fracture passing through the notch, but not why the fatigue fractures of notched specimens have been observed to be initiated at the edge of the specimen at the height of the notch, not from the notch. After the results, the main conclusions by the authors were (Johanson et al., 2018):

- The notch impact is higher on lower strain ranges. It also seems to be dependent on test frequency.

- The notch impact of the location of fracture initiation seems to be different for the two strain ranges tested. For the higher cyclic strain range the initiation fracture starts from the middle region of the specimen, both notched and un-notched. For the lower cyclic strain range, the failure only occurs in the middle region for notched specimens.

- The numerical calculations indicate that the highest strain concentration is at the notch, which justifies the reduction in fatigue life and change in failure location. However, usually, the final crack does not initiate at the notch, which means the test results appear to be inconsistent with the analysis.

- The lead alloy is expected to undergo irreversible deformation at the tested strain ranges, strain hardening, and local blunting can be mechanisms that cause redistribution of the strain and differentiates the monotonic and cyclic strain fields. This can explain a change in failure initiation.

- The material law used in this study as well as the DIC strain is collected from monotonic cases, the cyclic response will differ.

- As the power cable lead sheathings are tubular, the fracture initiation in the edges is a test artifact. The laboratory fatigue tests of test specimens are conservative compared to the real component. Care should still be taken when assessing fatigue life in ductile materials.

In the book "Lead: The Facts" by Thornton et al. (2001), as well as a lot of valuable information about the material properties of lead, some of the reasons why lead is used as sheath material is listed:

- It is completely impervious to water.

- It has very good corrosion resistance in a variety of media, including marine environments.

- It can be extruded in very long lengths, and also easily jointed by soldering

- It is pliable, so it can be coiled and uncoiled, without being damaged, during cable preparation, transport, and application.

- It can be applied to the cable core at temperatures which do not damage vital cable components.

In the article "The Fatigue Life of Lead Alloy E as a Sheathing Material for Submarine Power Cables" Anelli et al. (1988) performs an experimental investigation into the fatigue resistance of lead alloy E (an alloy E is a Pb-Sn-Sb alloy). The study carries out multiple tests with different temperatures. Even though the study shows the average number of cycles to failure is less when the temperature rises from 25°C to 75°C the conclusion is "Factors acting on the fatigue life such as temperature and grain size have been evaluated, but their effect is shown to be of minor importance for a properly manufactured cable sheath" (Anelli et al., 1988).

In the article "Fatigue of Lead Cable-Sheathing Alloys", Havard (1972) did a study with fatigue testing of lead alloys used for cable sheathing. The study concluded with "While a number of commonly used lead alloys are shown to have insufficient fatigue resistance, use of one of the recommended arsenical lead alloys will ensure 40 years of trouble-free service". He also concluded with "BS lead alloy E can be used in jacketed cables, except where the severe level of service strains at two cycles per day is applied. In unjacketed cables, it can be used where the load frequency is one cycle per day" (Havard, 1972).

Chapter 2

Theoretical Background

This chapter will present the relevant theory concerning lead, creep, fatigue, and mechanical testing. The theory will help build a good understanding of the topic before going forward with the fatigue testing.

2.1 Material

Lead was already a widely used material many centuries ago. It was utilized in water piping, engineering applications, and coins, among other things, either by itself or allied with other metals (Casas and Sordo, 2011). Due to its properties, lead is still an essential and highly used material to this day. Some of the properties that make lead a vital material is the low melting point and the resistance to corrosion in acidic environments (Guruswamy, 1999). Lead is used for various applications today, as storage batteries, for construction purposes, and cable sheathings. Due to the corrosion resistance, lead is utilized as sheathing for power cables in the petrochemical industry and subsea applications. As well as good corrosion resistance, lead is impervious to water and can be extruded in long lengths, as well as easily joined by soldering (Casas and Sordo, 2011).

As mentioned earlier, the lead is used as a sheathing material in power cables due to the physical properties of the material. Some of the properties of pure lead are listed in **Table 2.1**. The tensile strength of lead is only between 12-17 MPa, which means both steel, aluminum, and copper are stronger materials. It is common to add alloying elements to improve some of the properties of lead, the sheathing material investigated in this thesis is a Pb-Sb-Sn alloy. The low melting temperature indicates that creep behaviour occurs already at room temperature (Thornton et al., 2001), this will be discussed in section 2.3.

Density[kg/m^3]	Tensile strength[MPa]	Melting temperature[$^\circ$C]
11 340	12-17	327.5

Table 2.1: Properties of pure lead (Thornton et al., 2001).

2.2   Stress and Strain

When performing a tensile test, the results are often presented in a stress-strain curve. The specimen is often tested until rupture. The stress-strain curve illustrates the elastic and plastic behaviour of the material. The elastic part represents the elastic modulus of the material, which is a measurement of **(a)** how stiff the material is and **(b)** how the material's strength is versus deformation. The yield strength is the point where the deformation goes over to plastic deformation, and on the stress-strain curve, one can see the curve bends over. The strength of the material will continue to increase as the load increases until it reaches its maximum stress. This point is called the ultimate tensile strength. Beyond this point, necking starts, leading to rupture. The form of the stress-strain curve varies from material to material, depending on how brittle or ductile the material is (Dowling, 2012). A typical stress-strain curve is illustrated in **Fig. 2.1**.
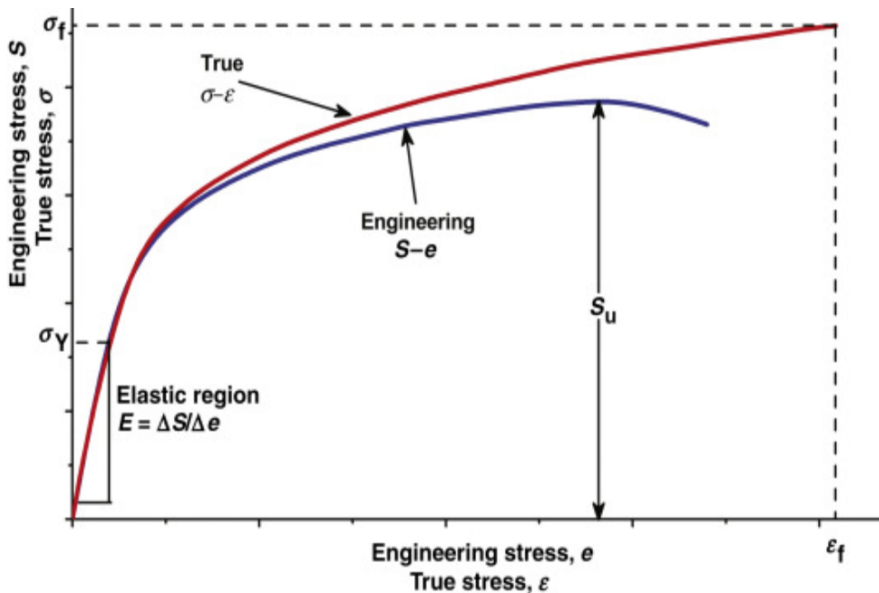
Figure 2.1: Typical stress-strain curve (McKeen, 2016).

It is possible to make two types of stress-strain curves: true and engineering. The most common is the engineering stress-strain curve, where the stress is calculated by dividing the force by the original cross-section. In this thesis, the true stress-strain curve is used. The true stress and true strain can be calculated by the use of engineering stress and strain,

which can be seen in Equation (2.1) and Equation (2.2). σ_0 is the engineering stress, σ is the true stress, e is the engineering strain, and ϵ is the true strain.

$$\sigma = \sigma_0 \cdot ln(1+e) \tag{2.1}$$

$$\epsilon = ln(1+e) \tag{2.2}$$

2.3   Creep

If a material experiences time-dependent plastic deformation under constant stress at elevated temperature, it is called creep. Creep is dependent on temperature and often occurs around 0.5 T_m, where T_m is the absolute melting temperature. For most materials, this means creep does not occur at room temperature. In lead however, the phenomenon occurs at room temperature due to the low melting temperature. When creep occurs, it can lower the strength of the material. This is difficult to measure because it needs to be tested by numerous tests over a long time period. For that reason, this is a relevant and important topic to study (Thornton et al., 2001). **Fig. 2.2** shows a schematic of a typical creep testing machine.
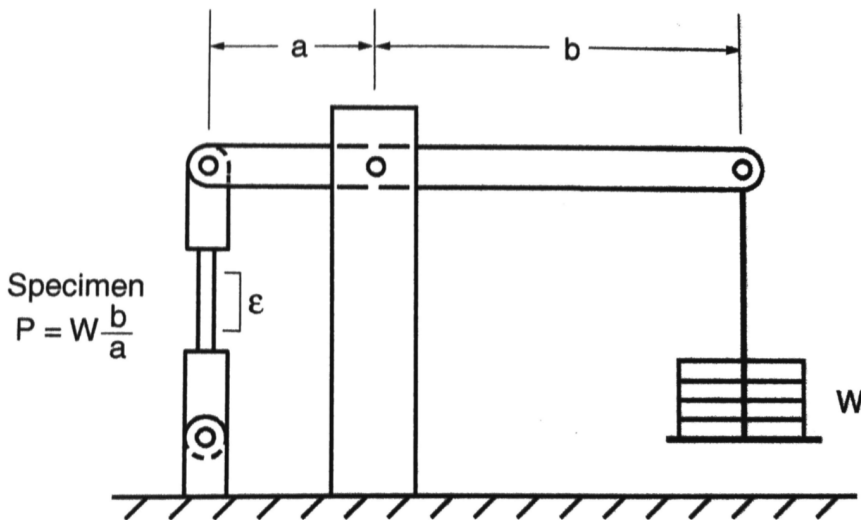
Figure 2.2: Schematic of a creep testing machine (Dowling, 2012).

When performing a creep test, a constant load or a constant strain rate is applied to the specimen, and the change of strain is recorded as a function of time. A creep test can be summarized by the three variables seen in Equation (2.3); σ, time, and temperature. $\dot{\epsilon}$ is the change of strain divided by the change in time Dowling (2012).

$$\dot{\epsilon} = f(\sigma, t, T) \tag{2.3}$$

$$\dot{\epsilon} = \frac{d\epsilon}{dt} \tag{2.4}$$

A typical creep curve shows three different stages: primary creep, steady state creep, and tertiary creep. An illustration of an idealized creep curve for constant load can be seen in **Fig. 2.3 (a)**. In the first phase, called primary creep, the creep rate decreases with increasing plastic strain. In this phase, the creep resistance of the material increases due to its deformation or strain hardening. In the second phase, called steady state creep, the creep rate is nearly constant and at its minimum. The close to constant creep is due to the balance of strain hardening and the recovery process. In the third phase, called tertiary creep, the creep rate increases with time, leading to fracture. The creep rate increases, not due to a change in loading, but as a result of a change in the cross-sectional area. When the tension is unchanged, the cross-sectional area will decrease, leading the stress to increase (Zhang, 2010; Guruswamy, 1999). **Fig. 2.3 (b)** shows a typical creep curve with three stages, where the strain rate is held constant. In the first stage, the flow stress increases with strain, due to metal hardening. In the second stage, the flow stress remains constant. Finally, in the third stage, the flow stress decreases until fracture (Zhang, 2010).
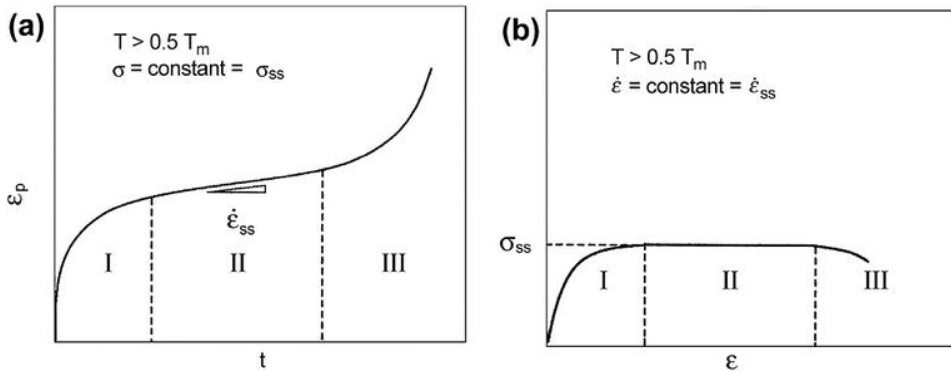
Figure 2.3: (a) Typical creep curve at constant stress and (b) typical creep curve at constant strain rate (Monfared, 2018).

Fig. 2.4 illustrates the results of two creep tests with constant strain rate. One can observe that the yield stress decreases significantly when the strain rate is decreased from $10^{-4}s^{-1}$ to $10^{-7}s^{-1}$. This indicates that creep in metals and alloys are highly strain rate dependent. As a possible approximation Kassner (2015) considers the microstructure at 0.002 plastic strain to be independent of $\dot{\epsilon}$. This means the decrease in yield stress illustrated in **Fig. 2.4** is only due to the change of strain rate and can be predicted by the stress-sensitivity exponent, N, which is defined in Equation (2.5). T refers to temperature and s refers to substructural features (Kassner, 2015).

$$N = [\frac{\partial ln\dot{\epsilon}}{\partial ln\sigma}]_{T,s} \tag{2.5}$$

For a creep test, the maximum stress in a constant strain rate test is referred to as the steady state stress. This steady state stress, σ_{ss}, that is achieved in a test with a constant creep rate
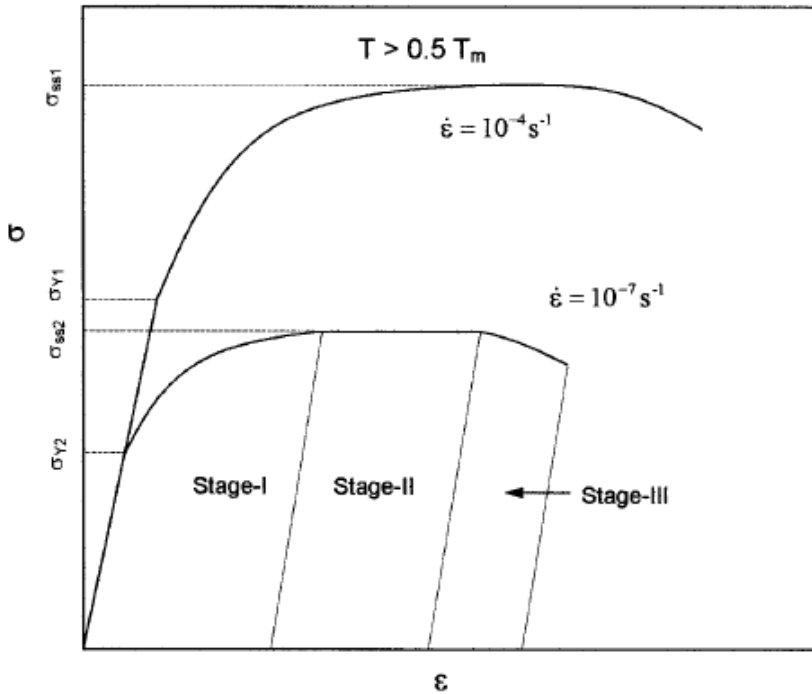
Figure 2.4: Creep at two different constant strain rates (Kassner, 2015).

at i.e $10^{-4}s^{-1}$, is the same stress that would achieve the strain rate $10^{-4}s^{-1}$ in a constant stress test. The variation of steady state creep rate with the applies stress can be described by the steady state stress exponent, n, which is defined in Equation (2.6) (Kassner, 2015).

$$n = [\frac{\delta ln\dot{\epsilon}_{ss}}{\delta ln\sigma_{ss}}]_T \tag{2.6}$$

Activation Energy

The activation energy for creep, Q_c, is a measurement of the energy barrier that needs to be overcome for creep to occur (Dowling, 2012). The activation energy is dependent on both the applied stress and the temperature. Q_c has often been found to be the same as the activation energy for self-diffusion of the metal, Q_{sd} (Kassner, 2015). Experiments by Campbell et al. (1987) on lead have shown that additions of Ag and Au that affect the self-diffusion appear to have the same effect on the creep rate (Campbell et al., 1987). **Fig. 2.5** illustrates the relation between Q_c and Q_{sd} for several metals, including lead. (Kassner, 2015).
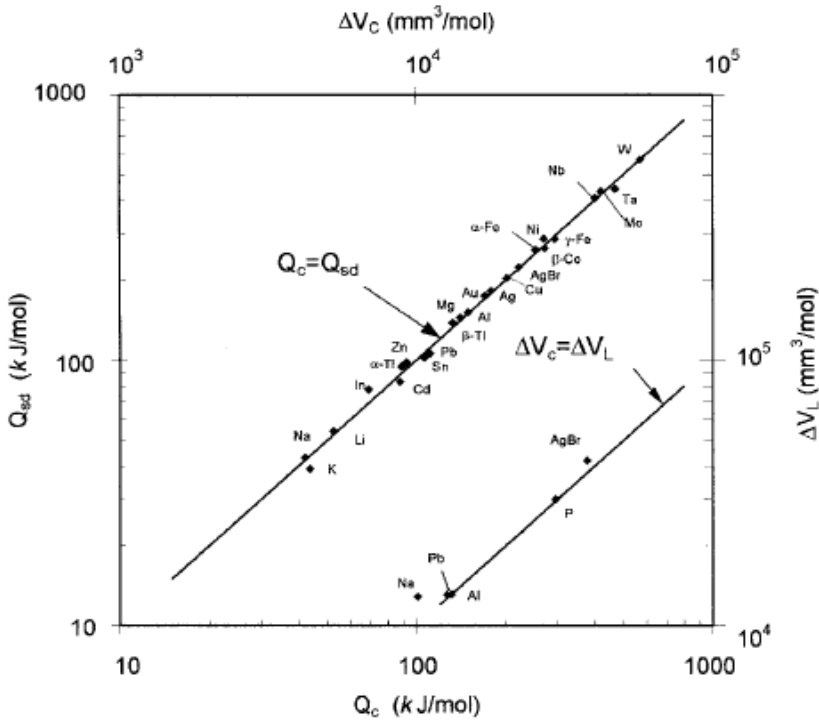
Figure 2.5: Relation between Q_c and Q_{sd} for a number of pure metals (Kassner, 2015).

2.3.1 Creep Mechanisms

A general equation for steady state creep rate in crystalline materials can be seen in Equation (2.7), where the factors influencing the creep rate are stress, temperature, grain diameter and activation energy, as well as the exponents *m* and *q*, which are dependent on the creep mechanism (Dowling, 2012). There are different mechanisms that contribute to creep in a material. The basic mechanisms are dislocation slip, climb, grain-boundary sliding and diffusion flow caused by vacancies (Pelleg, 2014). These mechanisms can along with a short description can be seen in **Table 2.2**. As well as the mechanisms mentioned in the table from Dowling (2012), Harper-Dorn creep will be discussed in this section.

$$\dot{\epsilon} = \frac{A\sigma^m}{d^q T} e^{\frac{-Q}{RT}} \tag{2.7}$$

Diffusional Flow

Both Nabarro-Herring- and Coble-creep are two methods of diffusion flow by vacancies (Pelleg, 2014). For diffusional creep to occur, two main conditions have to be fulfilled (Zhang, 2010):

Name of Mechanism	Description
Nabarro-Herring creep	Vacancy diffusion through the crystal lattice
Coble creep	Vacancy diffusion along grain boundaries
Grain boundary sliding	Sliding accommodated by vacancy diffusion
Power law creep	Dislocation motion, with climb over microstructural obstacles

Table 2.2: Creep Mechanisms (Dowling, 2012).

(i)   the stress has to be low enough
(ii)   the temperature has to be high enough

Nabarro-Herring creep is when the vacancies move through the crystal lattice, in other words lattice diffusion. The lattice diffusion in this mechanism occurs within the grain and causes the grains to elongate along the axis. Tensile stress induces the mass flow (diffusion of atoms). If on the other hand the vacancies moves along the grain-boundaries, it is called *Cobble creep*. Due to the material flow, the grain-boundary diffusion produces a change in dimensions. According to Dowling (2012), the creep exponents for the two mechanisms are: $m = 1$ for both and $q = 2$ for Nabarro-Herring and 3 for Cobble creep. Cobble creep often happens at lower temperatures compared to Nabarro-Herring creep, the dependence of stress is similar for the two mechanisms, but Cobble creep is more dependent on the grain size (Dowling, 2012). Both Cobble creep and Nabarro-Harring creep can happen at the same time, which means the creep rate can involve both (Pelleg, 2014). An illustration of the lattice diffusion that occurs in Nabarro-Herring creep and the grain-boundary diffusion that occurs in Cobble creep is illustrated in **Fig. 2.6**.
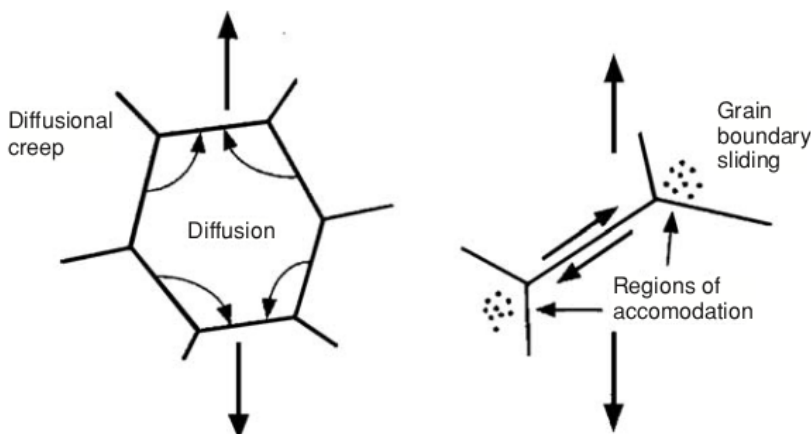
Figure 2.6: (a) vacancy flow; **(b)** flow along boundaries (Hosford, 2010).

Dislocation Creep

Dislocation creep, also called *power law creep*, is a creep mechanism that is not dependent on the grain size, and very dependent on applied stress. Dislocation creep relies on both glide and climb, which are two mechanisms illustrated **Fig. 2.7**. Dislocation slip occurs in primary creep. Glide-by-slip strengthens the material as they deform, by inducing strain hardening (Pelleg, 2014). As mentioned earlier, there is a balancing effect between strain hardening and the recovery process. The strain energy in the material is increased at this stage. This, together with high temperature, encourage the recovery process. This recovery process involves the rearrangement of dislocations into sub-grain boundaries. The dislocations have to climb or slip to move, which requires atomic movement or self-diffusion within the lattice (Pelleg, 2014).
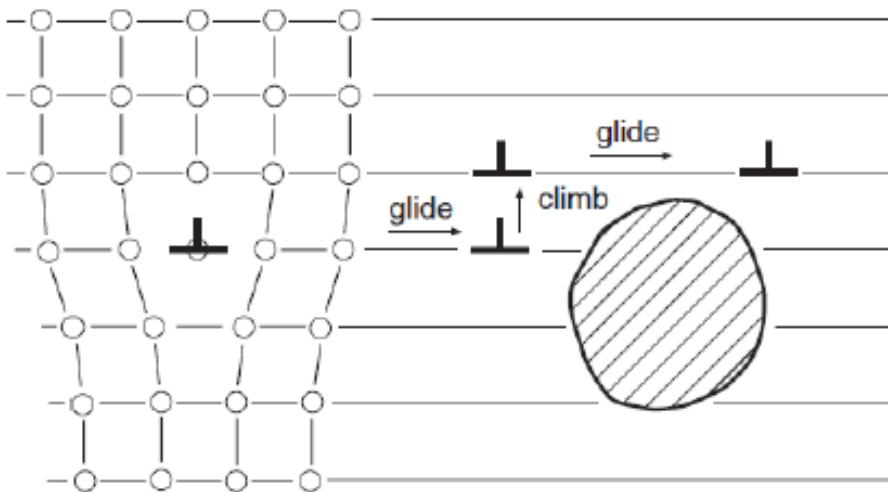
Figure 2.7: Climb and glide (Dowling, 2012).

Harper-Dorn Creep

Another creep method that is not as well known as the previously discussed methods is the *Harper-Dorn creep method*. In Harper-Dorn creep, the steady state strain rate increases proportionally with applied stress, $m = 1$, and it is independent of grain size. Because it is independent of grain size, it cannot be diffusional creep (Nabarro-Herring or Cobble creep). The activation energy for Harper-Dorn creep is the same as for diffusional creep, and the dislocation density is very low (Zhang, 2010). Harper-Dorn creep was first observed in aluminum and its alloys. Mohamed et al. (1973) tested if Harper-Dorn creep could be present in lead and they observed a creep behaviour that appeared to be Harper-Dorn creep.

Grain Boundary Sliding

Grain boundary sliding can occur both in diffusional creep and dislocation creep, in different ways. Grain boundary sliding involves the movement of grains and the process where grains slide past each other. This often happen in their common boundary. The grain size is an important variable in the microstructure of the material, and the movement in grain boundaries are important in the behaviour of materials experiencing creep (Pelleg, 2014). In diffusional creep, grain boundary sliding is an important coordinated mechanism, where both Nabarro-Herring and Coble creep has to be followed by grain boundary sliding to maintain the continuity of the material. During diffusional creep atoms are transported from the grain boundaries, leading to a change in the shape of the creeping grains. If grain boundary sliding does not occur after this process, voids will form on the grain boundaries subjected to compressive stress. In **Fig. 2.8** one can see an example by Raj and Ashby (1971) where grain boundary sliding occurs in two systems, perpendicular to each other (Zhang, 2010). In dislocation creep, grain boundary sliding does not need to happen. Grain boundary sliding does however still have a significant effect on the creep rate in dislocation creep when the grain size is smaller than 100μm. In that case, the creep rate increases with decreasing grain size (Zhang, 2010).
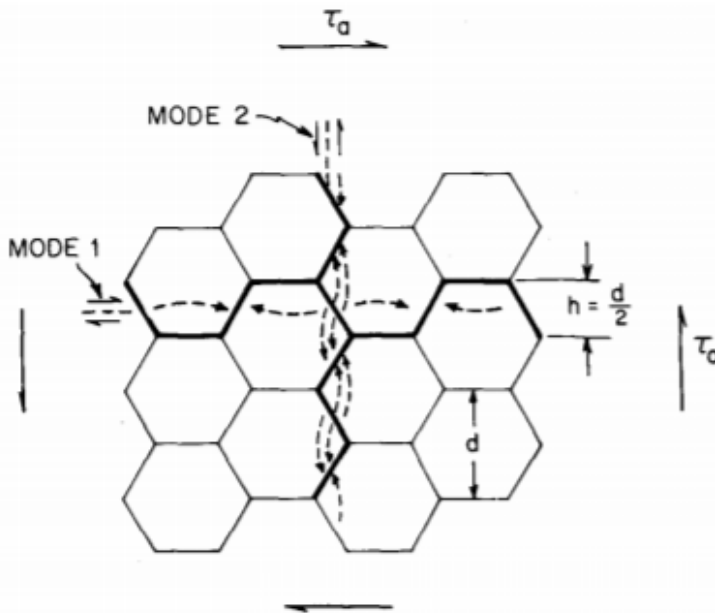
Figure 2.8: Grain boundary sliding into systems in an idealized polycrystal (Raj and Ashby, 1971).

Creep Mechanism Map

Among others, Langdon and Mohamed (1978) have written about a simple method of constructing an Ashby-type deformation mechanism map, which can be seen in **Fig. 2.9**.

One can observe where the different mechanisms mentioned above are observed. The thick lines on the map represent the boundaries between fields in stress-temperature space, while the thin lines are contours of two constant strain rates (Langdon and Mohamed, 1978). This is an approximation, and further tests for the relevant material is necessary.
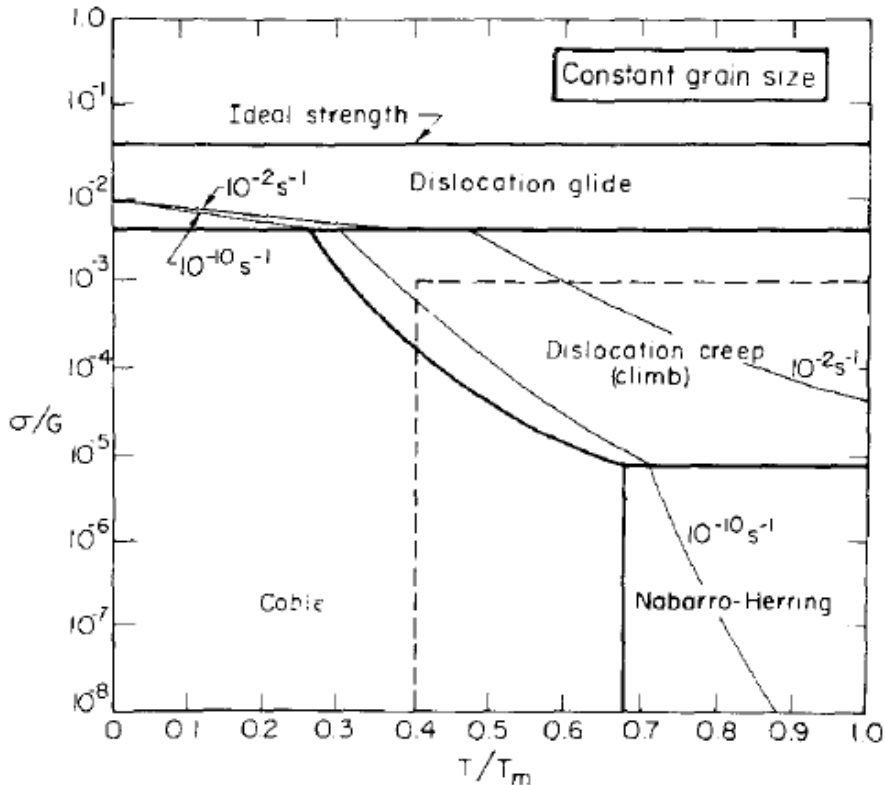
Figure 2.9: Schematic Ashby-type deformation mechanism map (Langdon and Mohamed, 1978).

2.4 Fatigue

When a component is subjected to frequently repeated loads, the resulting cyclic stress can lead to microscopic damages in the material. These damages can lead to failure even if the stresses are well below the ultimate tensile strength. This process where cyclic loading is the cause of damage and failure is called fatigue (Dowling, 2012). Fatigue failure can seemingly occur out of a sudden, with little plastic deformation. The failure is often initiated from a small notch or an irregularity due to stress concentrations. The fatigue process can often be divided into four stages: crack initiation, stage 1 crack growth, stage 2 crack growth, and ultimate ductile failure. How long each stage will last in the total fatigue life depends on the testing conditions and the material. Crack initiation is when the

crack first is being initiated, usually at a notch or discontinuities, which can occur already at 10% of the total fatigue life. Stage 1 crack growth is after the initiation when the crack propagates along slip planes. Stage 2 crack growth begins when the stress field at the crack tip becomes dominant. The crack then propagates in a direction that is normal to the applied tensile stress. The ultimate ductile failure occurs when the crack becomes so long that the cross-section remaining is not capable of carrying the load. When presenting the cyclic behaviour in a stress-strain curve, a hysteresis loop is gathered for each cycle. An example of a hysteresis loop can be seen in **Fig. 2.10** (Bhaduri, 2018).
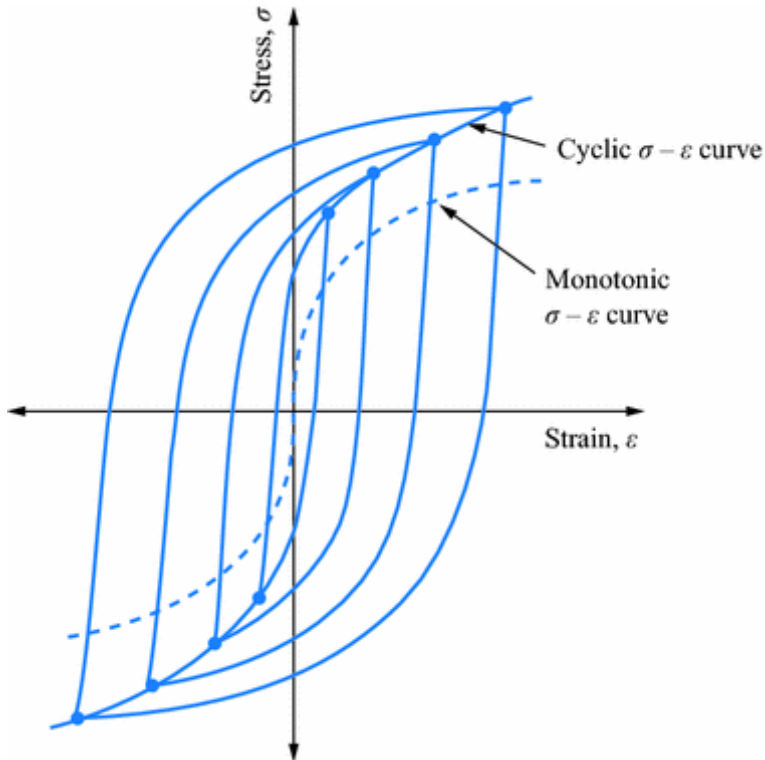
Figure 2.10: Schematic curves of monotonic and cyclic stress-strain for a material that cyclically hardens (Bhaduri, 2018).

Stress-Based versus Strain-Based Approach

When analyzing fatigue data, there are three main approaches: stress-based, strain-based, or fracture mechanics approach. The stress-based approach is based on analyzing the nominal stress versus life in the affected regions. The results are often plotted in a stress-life curve, with the stress amplitude S_a or σ_a versus the number of cycles to failure N_f. The strain-based approach is a more detailed way of analyzing local yielding that might occur. It considers the plastic deformation that could occur where fatigue cracks begin. The results are plotted in a strain-life curve, with the stress amplitude ϵ_a versus the number

of cycles to failure, N_f. The method gives improved estimates, especially for medium and short fatigue life. The fracture mechanics approach focuses on cracks growing, often plotting crack length, a, versus the number of cycles, N (Dowling, 2012).

2.4.1 Notch Effect

It is almost impossible to avoid any geometric discontinuities when designing a component, such as holes, grooves, or fillets. The discontinuities are often referred to as notches and cause the local stress to elevate. These notches can reduce the components fatigue life due to the locally increased stress. The **elastic stress concentration factor**, k_t, is the ratio between the local point stress and the nominal stress, it can indicate the severity of the notch. From looking at Equation (2.8), one might believe that the fatigue life for a smooth and a notched specimen, the stress $\sigma = S$ is the same as $\sigma = k_t S$ at the notch for the notched member. Tests have shown that the notch generally has a lower impact on the fatigue life than expected from looking at k_t. The **fatigue notch factor**, k_f is the actual reduction factor. k_f is defined for completely reversed stresses, as Equation (2.9) demonstrates. The radius of the notch has a big influence on the difference between k_f and k_t. If the notch has a big radius, the values might be almost equal, while for a smaller radius, the difference could be large (Dowling, 2012).

$$k_t = \frac{\sigma}{S} \tag{2.8}$$

$$k_f = \frac{\sigma_{ar}}{S_{ar}} \tag{2.9}$$

Looking at the notch effect, **notch sensitivity** is a useful concept. Equation (2.10) shows how it is calculated, where the value of q lies between 0 and 1. If the notch has maximum effect $k_f = k_t$ and q=1. The value decreases when $k_f < k_t$, where 0 is the minimum when $k_f = 1$. The value of q is therefore a good measure of how a specimen is affected by a notch. The notch sensitivity factor is dependent on the radius of the notch and the material. The notch sensitivity is greatest for highly ductile materials and sharp notches, and smaller for more brittle materials and blunt notches (Dowling, 2012).

$$q = \frac{k_f - 1}{k_t - 1} \tag{2.10}$$

Fracture Modes

When a specimen has obtained a crack or has a notch, it can be loaded in any one of three displacement modes, or a combination of two or three of them. The loading modes are described in **Fig. 2.11**. Mode I, is when the crack "opens". Mode II is when the crack faces slide in opposite directions. Mode III is when the crack tears open. When more than one mode is applied, it is called mixed-mode loading (Dowling, 2012).

2.4.2 Creep-Fatigue Interaction

Real-life components used in applications that operate cyclically experience both creep and fatigue at the same time. The load and temperature in the start-up stage of a cycle
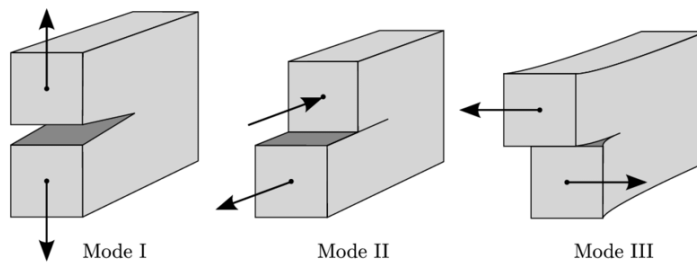
Figure 2.11: The three different basic modes of fracture (Kammer, 2014).

increase to the service condition. The component then experiences the steady loading conditions for a while, followed by the shutdown stage where the load goes to zero and the temperature back to room temperature. This means that the component suffers from fatigue damage from the start-up and shutdown of the operations and creep damage from the constant loading periods (Zhang, 2010). The interaction can be either creep enhanced by fatigue or fatigue enhanced by creep. This can also be seen on the fracture surfaces, as the creep fracture surface will have a tendency to intergranular fracture, and the fatigue fracture will have fatigue striations and regions of transgranular fracture (Bhaduri, 2018). Bhaduri (2018) has made a summary of when each of the situations occurs:

- Creep accelerated by fatigue is considered when:

    - Cyclic stress/strain amplitude is small compared to the mean stress/strain, or
    - Operating temperature is high, or/and applied cyclic frequency is low.

- Fatigue accelerated by creep is considered when:

    - Cyclic stress/strain amplitude is large compared to the mean stress/strain, or
   - Operating temperature is low or/and applied cyclic frequency is high.

As mentioned above, fatigue data is often presented in a hysteresis loop. **Fig. 2.12** is a schematic illustration of how the hysteresis loop can look like for a test with creep-fatigue interaction. One can observe how creep makes the curve inconsistent from the hysteresis loop illustrated in **Fig. 2.10**. Creep-fatigue damage is dependent on many parameters, such as creep ductility and creep strength and how it was strengthened - solid solution or precipitation strengthening, strain range, holding time and strain rate among others (Holdsworth, 2015; Zhang, 2010). **Fig. 2.13** illustrates four possible creep-fatigue cracking mechanisms. **(a)** and **(b)** are fatigue dominated and creep dominated, respectively. The main difference between these two is the hold time, where creep dominated is when the hold time becomes longer. **(c)** and **(d)** are both creep-fatigue interactions (Holdsworth, 2015).

Creep-Fatigue Failure Maps

As mentioned, there are many factors influencing the evolution of creep-fatigue damage. By considering the failure criteria as well as the damage initiation, the creep-fatigue failure
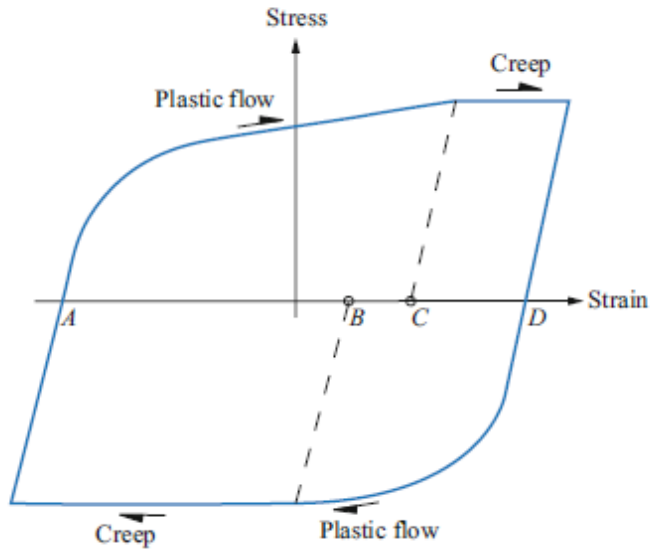
Figure 2.12: A hysteresis loop for a creep-fatigue interaction example (Bhaduri, 2018).
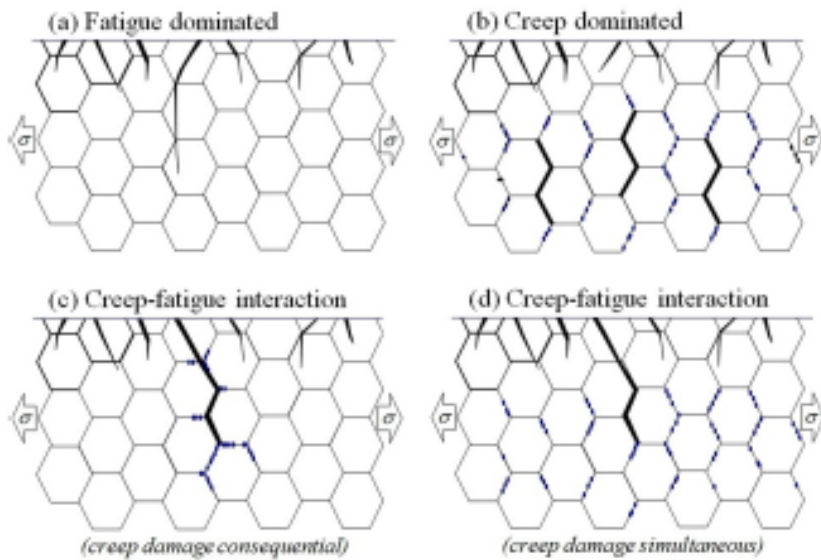
Figure 2.13: (a) fatigue dominated; **(b)** creep dominated; **(c)** creep-fatigue interaction due to consequential creep damage accumulation; **(b)** creep-fatigue interaction due to simultaneous creep damage accumulation (Holdsworth, 2015).

mapping technique was proposed. The mechanism map can be seen in **2.14**, which is a two-dimensional section at a given hold time. Here one can see four curves representing creep initiation, creep failure, fatigue initiation and fatigue failure as labeled on the figure (Zhang, 2010).
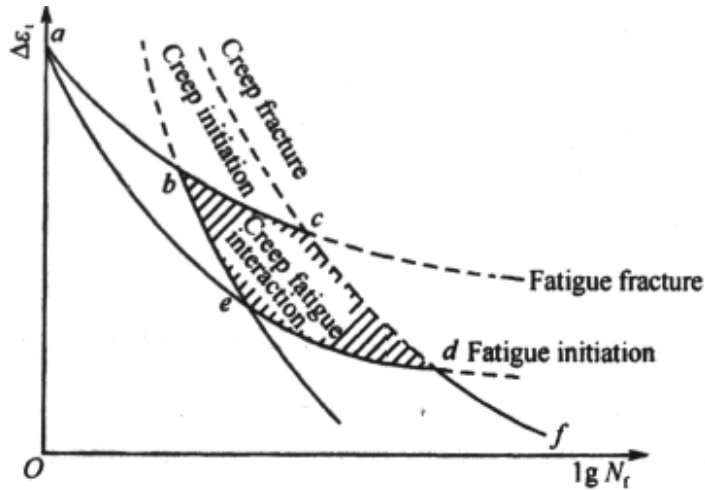
Figure 2.14: Schematic creep-fatigue mechanisms map (Zhang, 2010).

2.5 Mechanical Testing

When deciding the mechanical properties of a material, numerous tests can be performed. These tests can measure the strength, the hardness, or any other property of interest. Some of the common tests are bending, tension, compression, or torsion tests (Dowling, 2012).

2.5.1 Tensile Testing

Tensile tests are performed in order to determine the material properties of a specimen. A load displacement is applied to the specimen, and it deforms until fracture by increasing the load in the same direction as the movement. Machines made for tensile testing measure the applied load, elongation, and strain rate. The test specimen is an important factor when performing a tensile test, and in **Fig. 2.15** a typical test specimen is illustrated. The shoulder on each side is important because of the grip from the test machine. The gauge length is where the actual deformation and fracture is happening, and the gauge length should be long compared to the diameter. The output of a tensile test is a stress-strain curve, as mentioned in Section 2.2 (Hosford, 2010).
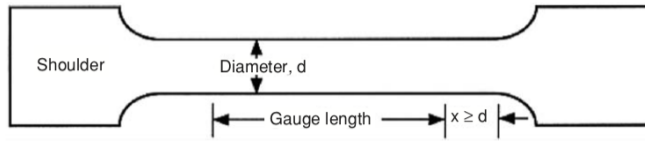
Figure 2.15: A typical specimen for tensile testing (Hosford, 2010).

2.5.2 DIC

Digital image correlation is a strain measuring technique, which is used in this thesis. DIC compares digital photographs of a specimen at different stages of deformation, this means it measures deformations without contact (McCormick and Lord, 2010). It is possible to use DIC in 2D and 3D, with two cameras used for the latter. This thesis will only focus on 2D DIC due to a time limit. The 2D DIC method is limited to in-plane deformation, which means if the specimen ends up being bent after deformation, the results from 2D DIC is not applicable (Pan et al., 2014). According to Pan et al. (2014) implementation of the method consists of three steps:

1. Specimen and experimental preparation

2. Taking images of the planar specimen surface before and after loading

3. Post-processing by utilizing a numerical computing software

A typical setup for 2D DIC is illustrated in **Fig. 2.16**, where the camera is set up normal to the specimen. In order to track the deformation of the specimen, it has to have a random
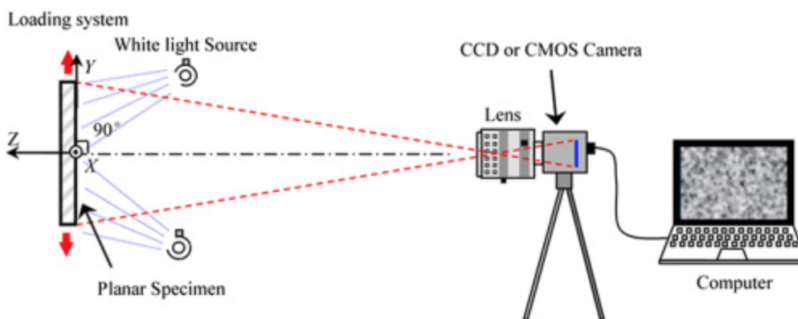
Figure 2.16: Schematic example setup for 2D DIC (Pan et al., 2014).

speckle pattern, naturally or painted. The pattern deforms together with the specimen, and the post-processing software can obtain the movement of the speckles. This will result in finding the strain and deformation in the material (Pan et al., 2014). Three examples of the speckled pattern can be seen in **Fig. 2.17**.
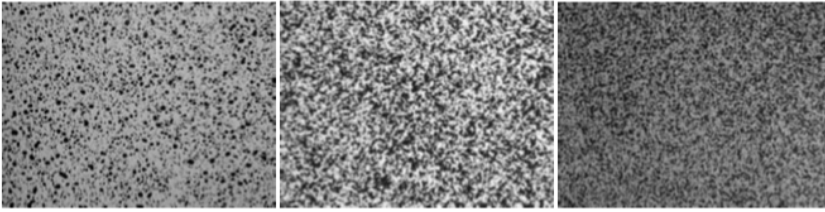
Figure 2.17: Examples of typical speckle patterns (Schreier et al., 2009).

Some of the **advantages** of using 2D DIC listed by Pan et al. (2014) are:

- It is easy to set up the method, only needing a camera and the specimen with speckles.

- The light required is not a laser source, but regular white light or natural light.

- The resolution and measurements can vary after what is needed.

There are some **disadvantages** as well, according to Pan et al. (2014) some of them are:

- The specimen has to have the speckled surface.

- The quality of the images is crucial for a reliable result.

- The accuracy of the strain measurement is not as high as other techniques.

Post-Processing

The software utilized for post-processing the material captured by the DIC is eCorr v4.1, which is a numerical computing software developed by Egil Fagerholt (Fagerholt, 2017). The numerical program uses the speckles on the specimen to evaluate the movement of the specimen and to compute the strain and displacements. The software uses a reference picture from before the load was applied, then the pictures through the deformation. In **Fig. 2.18** there is a schematic illustration of how post-processing work, and how the software uses the speckles to find the strain and displacements.
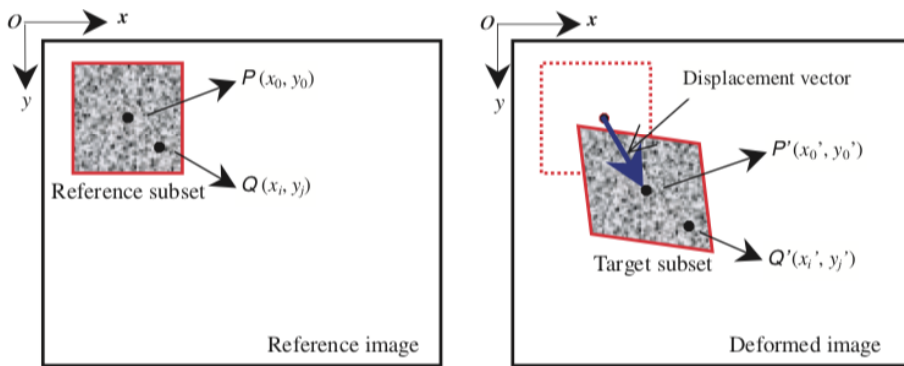
Figure 2.18: Schematic illustration of how the software processes the DIC material (Pan et al., 2014).

Material Calibration

This chapter will go through the experimental results, the finite element modeling, and the material calibration resulting in a material model. By utilizing experimental results from fatigue testing of material cut directly from lead sheathings, a material model will be calibrated to replicate the material's behaviour. The lead sheathing material and all the test specimens used in this thesis is a Pb-Sn-Sb alloy, also called lead alloy E.

3.1 Background

Material calibration is the process whereby utilizing the results from experimental and numerical testing; one can obtain a material model that describes the behaviour of the material. The softwares applied in this thesis were Abaqus for the finite element analysis and Isight for the material calibration. The material calibration will result in a material model that will be utilized to obtain a solid understanding of the impact of irregularities in the material in the following chapters. The material calibration has been performed on the results from fatigue tests conducted on specimens with no irregularities. The geometry of the specimen that has been tested can be seen in **Fig. 3.1**. This is a specimen cut from a cable sheathing, which will give results closest to reality. The thickness of the specimen is 1.8mm. The fatigue tests of both the numerical and experimental testing were performed with different strain rates: $1\text{E-}4s^{-1}$, $1\text{E-}3s^{-1}$ and $1\text{E-}2s^{-1}$. It was necessary to conduct tests at different strain rates to compare the results due to the high strain rate dependency of the material.

3.2 Experimental Test Results

The experimental testing was conducted by Nexans and SINTEF, and the results can be seen in **Fig. 3.2**. Digital image correlation was used to obtain the results from the experimental testing, which was explained in Section 2.5.2. One can see how the results from the different strain rates are different due to the strain rate dependence of the material. To
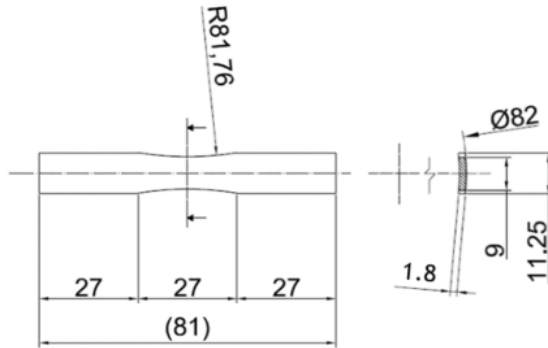
Figure 3.1: Geometry of the model used for material calibration.

ensure that the experimental results were applicable for the calibration, Ramberg-Osgood equation, Equation (3.1), was applied to provide curves for each of the three strain rates (Dowling, 2012). In the equation k' and n' are constants that needed to be found, which was different for each strain rate. E is Young's modulus, which for these tests are found to be 15000 MPa. **Fig. 3.3** illustrates the curves, as well as the initial results. The data for this can be seen in Appendix A.

$$\epsilon = \frac{\sigma}{E} + \left(\frac{\sigma}{k'}\right)^{\frac{1}{n'}} \tag{3.1}$$

3.3   Numerical Testing

The software used for numerical simulations by finite element method (FEM) is Abaqus. The main purpose of these finite element analysis (FEA) was to compute cyclic tests to compare with the results from the experimental tests and to calibrate a material model that describes the fatigue behaviour of the material, with no irregularities.

Model

As can be seen in **Fig. 3.1**, the geometry of the specimen contains symmetry, and it was only necessary to model one fourth of the geometry in Abaqus. This makes the process of meshing and the simulations both easier and faster. The model, as can be seen in **Fig. 3.4**, is a three dimensional solid with a thickness of 1.8mm. The dimensions can be seen in Appendix B. For the finite element models, the step time and increment size had to be assigned. The calculation of step times can be seen in Equation (3.2), where the value varies for different strain rates. The complete list of step times and strain rates that were tested in this thesis can be seen in **Table 3.1**. The average strain rate was, and the planned strain rate is not exactly the same, but for simplicity, the tests will be referred to with the
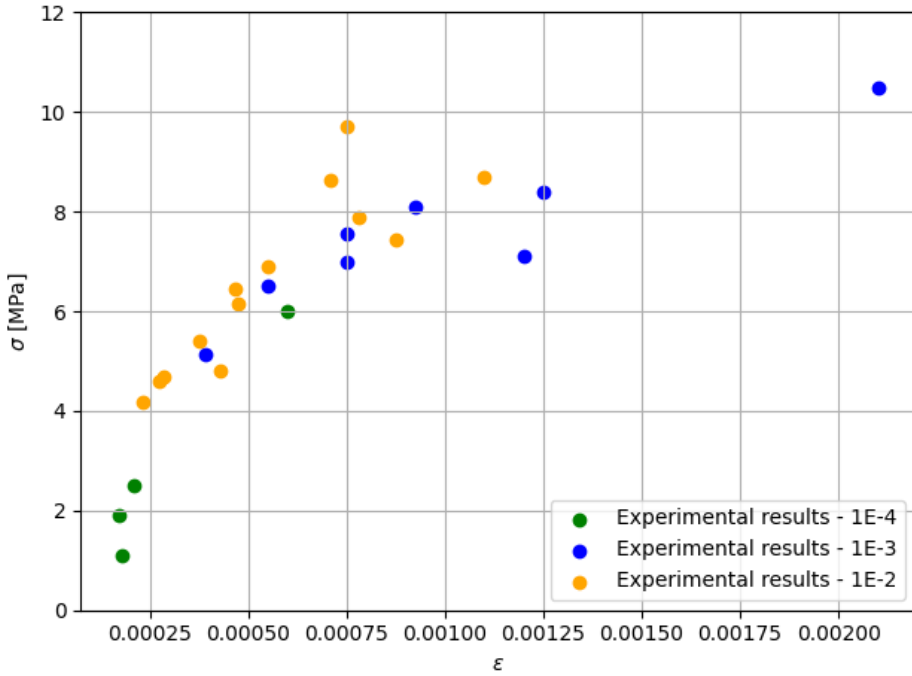
Figure 3.2: Results from experimental testing of a smooth specimen.

planned strain rate. In the finite element models, the average strain rate has been applied.

$$\triangle t = \frac{\triangle \epsilon}{\dot{\epsilon}} \tag{3.2}$$

Planned strain rate	Average strain rate	Step time
1E-4s^{-1}	0.00522602s^{-1}	60s
1E-3s^{-1}	0.000614123s^{-1}	4.9s
1E-2s^{-1}	0.00005s^{-1}	0.6s

Table 3.1: Strain rate and step time for the numerical simulations.

Material Properties

In the property module, the material had to be assigned the specimen. This was necessary for: elastic properties, plastic properties and creep properties.

The elastic properties are given in **Table 3.2**. Young's modulus was obtained from the
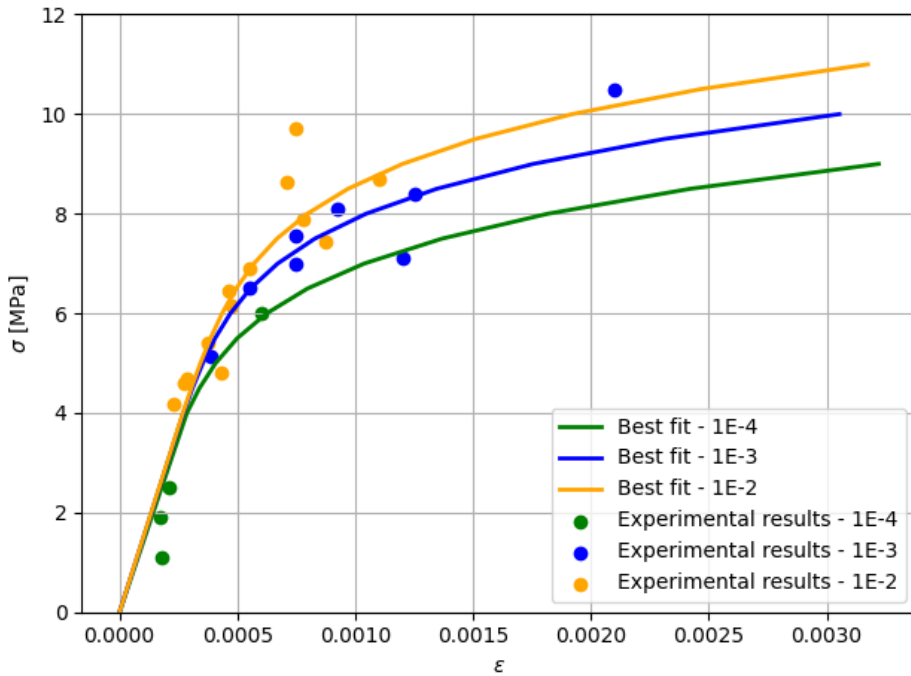
Figure 3.3: Best fit curves from experimental testing, constructed by the Ramberg-Osgood equation.

experimental tests, by considering a modulus that fit all the three strain rates, and Possion's ratio was obtained from Viespoli et al. (2019c).

Young's modulus [MPa]	Poisson's ratio
15000	0.431

Table 3.2: Elastic properties obtained from Viespoli et al. (2019c) and experimental tests.

The plastic properties had to be estimated using the results from the experimental testing. The plastic curve was computed from the $1\text{E-}2s^{-1}$ curve from the experimental results, after multiple iterations in Isight to obtain the best fit for the final material model. The data can be seen in Appendix C.

The creep model used in these simulations is the *power law model*, which was explained in Section 2.3.1. The equation for the power law creep model can be seen in Equation (3.3), where (Viespoli et al., 2019c):

- $\dot{\tilde{\epsilon}}^{cr}$ is the uniaxial equivalent creep strain rate.

- $\tilde{q}$ is the uniaxial equivalent deviatoric stress.
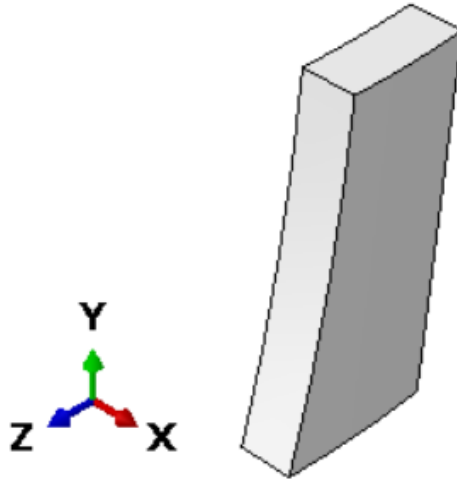
Figure 3.4: Abaqus model with no irregularities.

- A, n and m are constants that has to be calibrated to get the right creep behaviour.

$$\dot{\epsilon}^{cr} = (A\tilde{q}^n[(m+1)\epsilon^{cr}]^m)\frac{1}{m+1} \tag{3.3}$$

Viespoli et al. (2019c) has fitted the constants for the power law model for a tensile test and these results are the values applied as starting values for this thesis. The material calibration will produce new values that suit the cyclic loading that are tested. The start values for the relevant material properties can be seen in **Table 3.3** (Viespoli et al., 2019c).

Thickness[mm]	E [MPa]	ν	A	n	m
1.8	15000	0.431	7.27818E-10	5.10577	-0.389647

Table 3.3: The start values for the power law model (Viespoli et al., 2019c).

Boundary Conditions

As the model only comprises one fourth of the original specimen, two sides are constrained with symmetry. The direction of the deformation is in the negative y-direction, with a magnitude of 0.035mm. See equation (3.4) for the calculation, where the deformation equals the strain multiplied with the length of the specimen. Because the model represents cyclic loading, the dislocation was applied with an amplitude, going from t=0 to t=step

time, with the amplitude going from 0 to 1. The model was locked in the x-direction, this was to prevent any movement in that direction or false results. The model with the applied boundary conditions can be seen in **Fig. 3.5**, while **Table 3.4** gives an overview over the boundary conditions.

$$\delta = l \cdot \epsilon = 13.5mm \cdot 0.0025 = 0.034mm \approx 0.035mm \tag{3.4}$$

Boundary condition	X	Y	Z
Symmetry	-	U2 = UR1 = UR3 = 0	U3 = UR1 = UR2 = 0
Displacement/rotation	0	-0.035	-

Table 3.4: Boundary conditions for the Abaqus model.
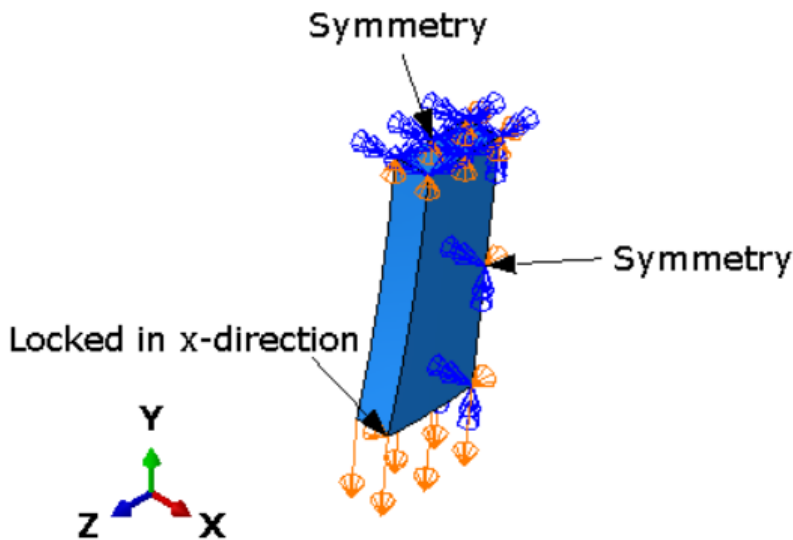
Figure 3.5: Abaqus model with applied boundary conditions.

Mesh

Sommacal (2018) conducted a convergence study to investigate the use of element type and element size for the same material as in this thesis, the results showed it was sufficient with C3D8R elements and a global size of 0.6. The model was therefore meshed with

C3D8R elements, this is displayed in **Fig. 3.6**. The global size used for this model is 0.25.

Figure 3.6: Abaqus model with applied mesh and the element from where stress and strain are extracted from the model.

Output Requests

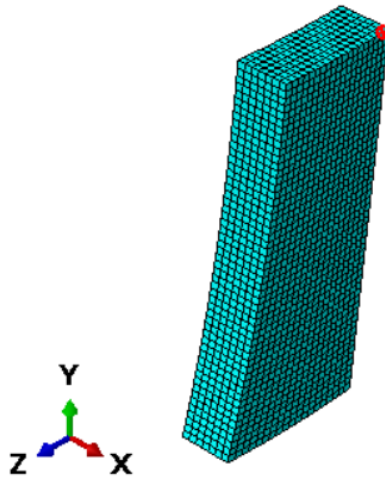The field output requests were stresses, plastic strains, creep strains, logarithmic strains, translations, and rotations. The history output requests were all energy totals, stress, and strain in the z-direction. The field- and history output requests had to be extracted from an element that would resemble how the results from experimental tests are gained. The element chosen can be seen in **Fig. 3.6**.

3.4 Isight

To ensure that the FEM simulations that are conducted accurately replicate the material's behavior, the material model has to be suited for the relevant usage and properly calibrated. In this case, the material model must replicate the behaviour of the material during cyclic loading. Isight was utilized to calibrate the parameters of the creep model. As the material is highly strain rate dependent, a sim-flow optimization was conducted, the sim-flow is illustrated in **Fig. 3.7**. The optimization uses Abaqus simulations that represent the different strain rates for the numerical results along with "data matching" with the experimental results. The goal is to obtain a model that fits all of the strain rates as good as possible. This can be done by different statistical measures, such as relative error, the sum of the squared difference, and so on. Experimental results used in data matching, are the best fit-curves

shown earlier. An example of this, for the tests with strain rate of 1E-2s^{-1}, can be seen in **Fig. 3.8**. The black curve in the figure represent the best fit-curve from experimental results and is the target. The red curve represents the FEA results from Abaqus. The goal would be for those curves to be as equal as possible for all of the three strain rates.
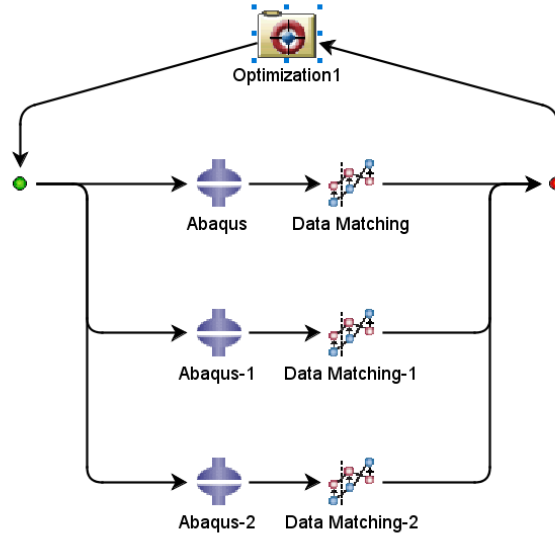
Figure 3.7: Isight sim-flow for the optimizing of the power law constants.

The Power Law

The creep model utilized for this thesis is the power law. The equation used for this can be seen in Equation (3.3), where n, m and A are material parameters. As there are only three parameters that need to be calibrated for this model, the Hookes-Jeeves algorithm was utilized. This is due to its ability to find a precise solution by exploring one parameter each run (Dassault Systems, 2017). In the data matching component, the three measurements: the sum of square difference, the sum of the absolute area difference, and the maximum difference were applied. The goal is to minimize the error for all of the three strain rates, as the material model needs to fit all for correct results.

Results

The optimization resulted in the parameters that can be seen in **Table 3.5**. The parameters were applied in the finite element models in Abaqus, to obtain the results. The comparison between the experimental and numerical results can be seen in **Fig. 3.9**. One can observe that the fit is good for all the three strain rates, this indicates that the use of the power law creep model was appropriate and that it was sufficient to use Hooke-Jeeves as optimization
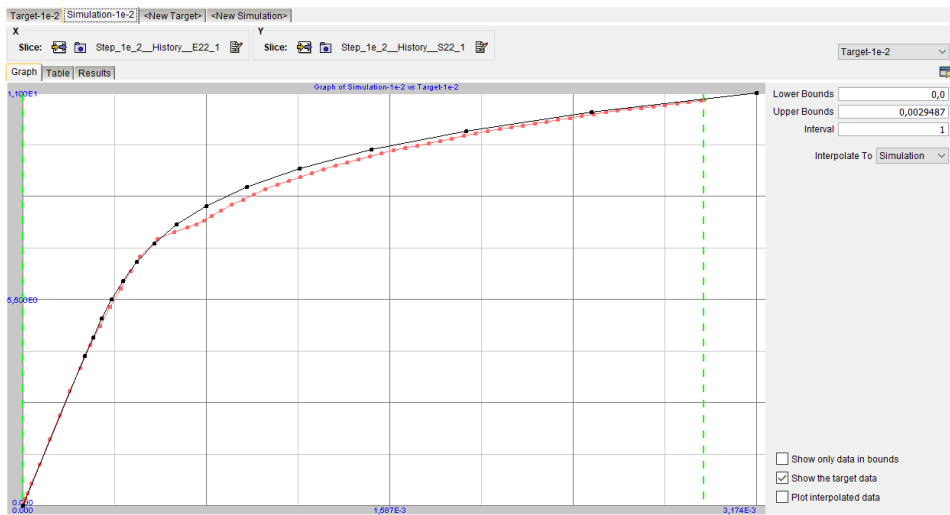
Figure 3.8: An example of the data matching between experimental and numerical results for one of the strain rates in Isight.

technique. The results are satisfactory, and it is reasonable to continue with the parameters. The creep model parameters will be applied in the investigation of the notch impact on fatigue life.

A	n	m
2.00625E-07	3.24735	-0.62912

Table 3.5: Results from optimizing the parameters of the power law creep model.
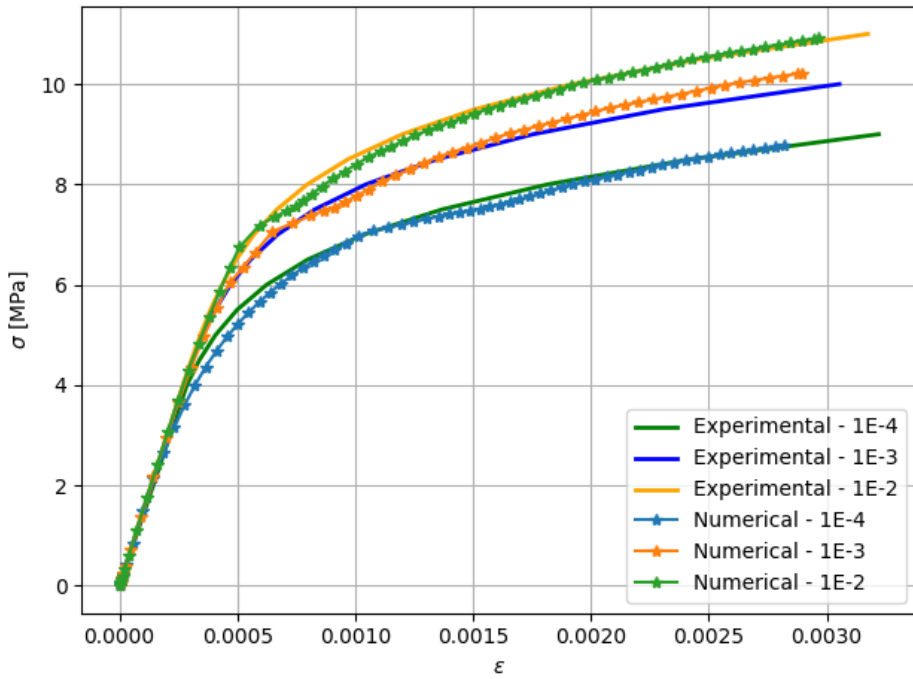
Figure 3.9: The experimental results and the results from Abaqus after the material calibration compared.

Chapter 4

Procedure for Fatigue Testing

The irregularity impact has been investigated by conducting fatigue tests on smooth and notched specimens. This chapter contains setup and procedure for fatigue testing of smooth and notched specimens, both experimental and numerical results are used. The maximum equivalent strain and the nominal strain have been extracted to get a deeper understanding of the irregularity impact on fatigue life. The finite element model utilized for material model calibration in Chapter 3 has been used, as well as a new finite element model for the notched specimen. The results of the analysis are presented in Chapter 5.

4.1 Experimental Data

The experimental data used in this chapter were carried out by SINTEF. They have been obtained by performing cyclic tests and using DIC to extract the results. Tests were conducted on specimens with and without irregularities and with two different strain rates, 1E-3s^{-1} and 1E-2s^{-1}. There were six tests for each strain rate of the notched specimens, where the global strain range differed from 0.1% to 0.2%. 17 smooth specimens were tested with a strain rate of 1E-2s^{-1}. They were tested to a global strain range of 0.1% to 0.25%. Out of these 17 specimens, three tests experienced some kind of error, six tests were run outs and the remaining eight tests failed after a certain number of cycles. There were ten smooth specimens tested with a strain rate of 1E-3s^{-1} and a global strain range of 0.1% to 0.25%, where two of the tests were run outs and the remaining eight failed after a certain number of cycles. The results from all of these tests are the base of the investigation that will be explained in the following sections. The main findings that will be utilized is the local nominal strain range and the number of cycles until failure. The way the nominal strain range was obtained in the DIC post-processing differed for the smooth and notched specimen, and will also be explained.

4.2   Finite Element Model of the Notched Specimens

For the experimental testing, there were several models with irregularities. All the speci-
mens were cut out of a lead cable sheathing. The irregularities had the same shape, with
different values. The goal was to look into the impact on fatigue life generally, not just for
one specific irregularity, it was therefore decided that the most expedient way to obtain the
best results was to make one model with average values. **Fig. 4.1** illustrates the general
geometry for the models and the average parameters that are used can be seen in **Table
4.2**. From observing the real specimens one could see that the irregularity was more like
a smooth notch, which was how the model was made in Abaqus. This models contains
symmetry, and therefor only one forth of the specimen is modeled. The model, which can
be seen in **Fig. 4.2**, has two curves making a blunt notch, resulting in the thickness being
1.8mm and the parameter m being 0.17mm. The full geometry of the model can be seen
in Appendix D. The fatigue testing has been conducted with the strain rate of 1E-3s^{-1} and
1E-2s^{-1}, where the step times are listed in **Table 4.1**.

Strain rate	Step time
1E-3s^{-1}	30s
1E-2s^{-1}	3 s

Table 4.1: Strain rate and step time for the numerical fatigue simulations.
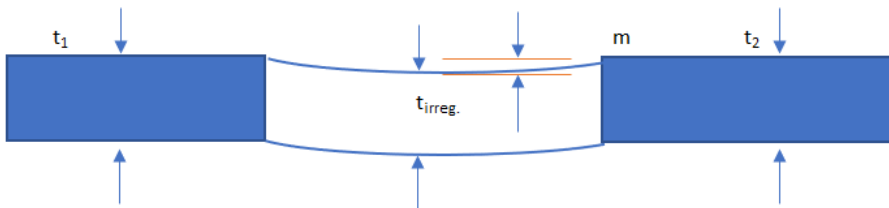
Figure 4.1: The general shape of irregularities on the specimen.

m	t_1	t_2
0.17mm	1.8mm	1.8mm

Table 4.2: Parameters for the model with irregularities.

Material Properties

The material properties assigned to the model, are from the calibrated material model in
Chapter 3. **The elastic properties** are given in **Table 3.2**. **The plastic properties** are
given in Appendix C. **The creep model** used is the power law model, with the equation
given in Equation (3.3). The parameters used are listed in **Table 3.5**.
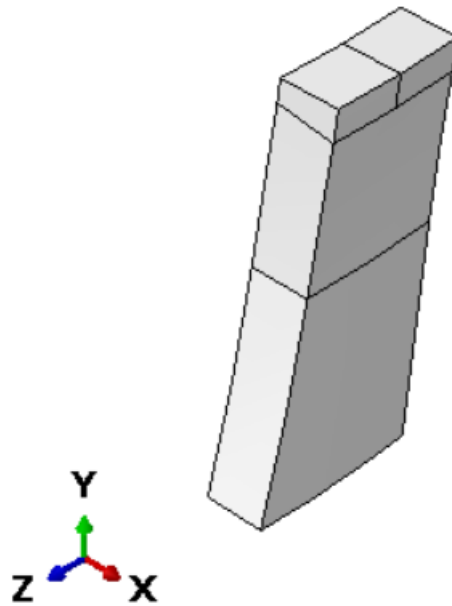
Figure 4.2: Abaqus model with irregularities.

Boundary Conditions

The models with irregularities have been applied with the same boundary conditions as the original model. To be able to compare the results, the two models have to be tested under the same conditions. The boundary conditions are summarized in **Table 3.4**, where the displacement in y-direction is applied as cyclic loading. The model with the applied boundary conditions can be seen in **Fig. 4.3**.

Mesh

The model was meshed with the same element type as the smooth model, C3D8R. Due to the irregularity, it was necessary to partition the model before meshing. The global size for this model is 0.2, this was done to get a mesh that does not influence the strain distribution and stress concentrations. The entire model with applied mesh can be seen in **Fig. 4.4a**. Due to the irregularity, some parts of the mesh were not hex elements, which this is visible in **Fig. 4.4b**. The mesh was verified in Abaqus with no warnings, the mesh was therefore accepted.

4.3 Output Requests

To ensure that the fatigue data from both of the models are comparable, it is important to consider how the outputs are extracted. The experimental data obtained by DIC used
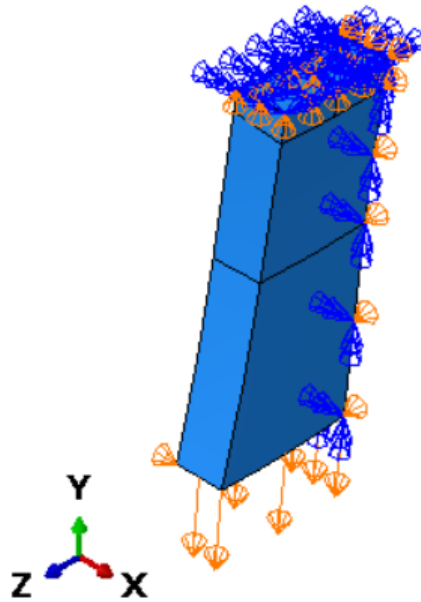
Figure 4.3: Abaqus model with irregularities, with applied boundary conditions.

different methods for the ones with irregularities and the ones without irregularities. **Fig. 4.5a** illustrates that strain is extracted from a short vector in the middle of the smooth specimen. If the same method would be used on the notched specim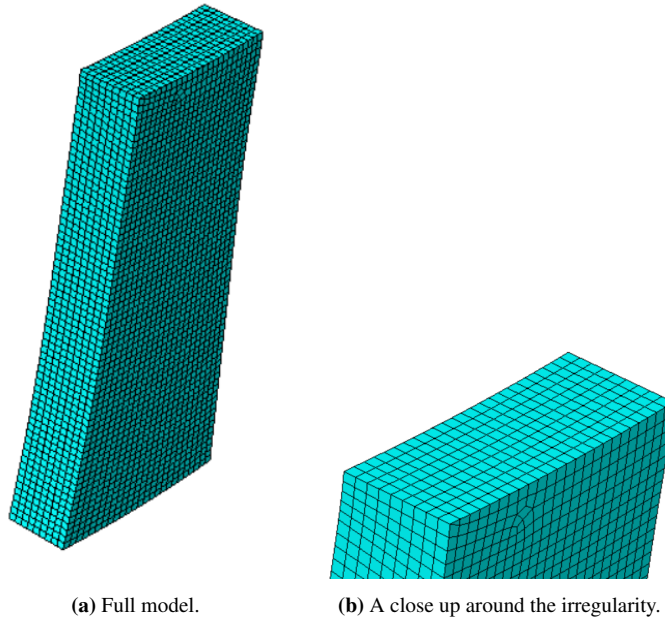en, the results would be more imprecise. By looking at **Fig. 4.5b**, a specimen with irregularities, one can see the strain is obtained by the use of three long vectors. This is to get the most genuine results, because of the irregularities and how it affects the strain distribution. These differences makes the process of extracting the results unlike.

4.3.1   Equivalent Strain in the Worst Point

Fig. 4.6 illustrates the strain distribution for the models with and without irregularities. One can observe that the distribution is different for the two models, due to the irregularity. As expected, the point with the highest strain is the same in both models. To compare the results, the equivalent Von Mises strain in the worst point was used. The equation for this can be seen in Equation (4.1) and Equation (4.2), where $\gamma_{ij} = 2 \cdot \epsilon_{ij}$ (DIANA, 2012). One can obtain ϵ_{ij} directly from Abaqus, by creating a history output from the chosen element. The elements that were used can be seen in **Fig. 4.7**.

$$\epsilon_{VM} = \frac{2}{3} \cdot \sqrt{\frac{3 \cdot (\epsilon_{xx}^2 + \epsilon_{yy}^2 + \epsilon_{zz}^2)}{2} + \frac{3 \cdot (\gamma_{xy}^2 + \gamma_{yz}^2 + \gamma_{xz}^2)}{4}} \tag{4.1}$$

$$\gamma_{ij} = 2 \cdot \epsilon_{ij} \tag{4.2}$$

(a) Full model. (b) A close up around the irregularity.

Figure 4.4: The Abaqus model with applied mesh.

The results from the experimental test were given in percentage of $\triangle\epsilon$. To ensure the results for the smooth and notched specimens were comparable, the way to determine at which time step the strain should be measured at was different. For **the smooth specimen**, the vectors used in the DIC post-processing were short and in the center. Equation (4.3) demonstrate how the strain in the longitudinal direction in the center element shown in **Fig. 3.6** was calculated. The time step where ϵ_{yy} equals ϵ_{abacus} is the time step where the parameters to fill into the equivalent Von Mises equation are gathered.

$$\epsilon_{abacus} = \frac{\triangle\epsilon}{2 \cdot 100} \tag{4.3}$$

It would give the wrong results if the same method was applied for **the notched specimen**. For the notched specimen, the vectors used in the DIC post-processing were long. The displacement of a node placed at the end of the long vector was used instead, which can be seen in **Fig. 4.8**. The magnitude of the displacement in the longitudinal direction was calculated as illustrated in Equation (4.4). The long vector was estimated to be 22mm. As for the smooth specimen, the time step where U_y is equal to $displacement_{abacus}$ is the time step where the parameters to fill into the equivalent Von Mises equation are gathered.

$$displacement_{abacus} = \frac{\triangle\epsilon \cdot l_{vector}}{2 \cdot 100} \tag{4.4}$$

(a) Model without irregularities.

(b) Model with irregularities.
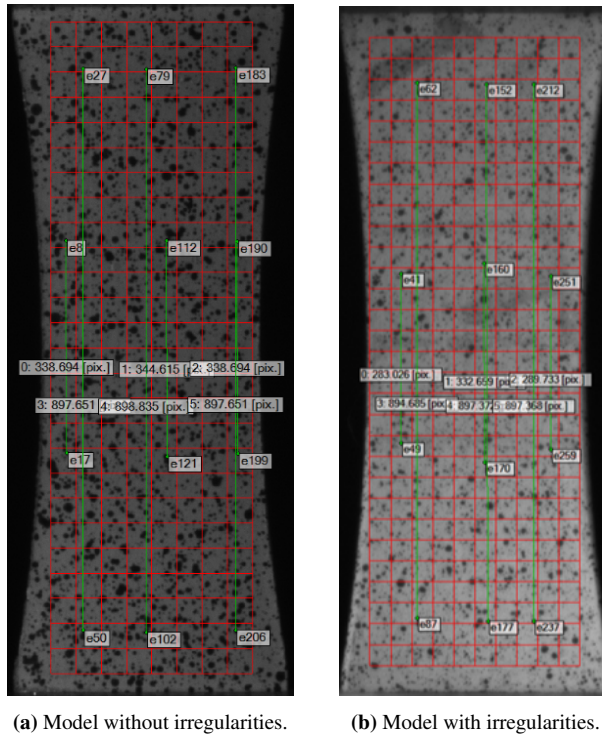
Figure 4.5: An illustration of the vectors used to extract strain from the models utilizing DIC and DIC post-processing.

(a) Model without irregularities.

(b) Model with irregularities.
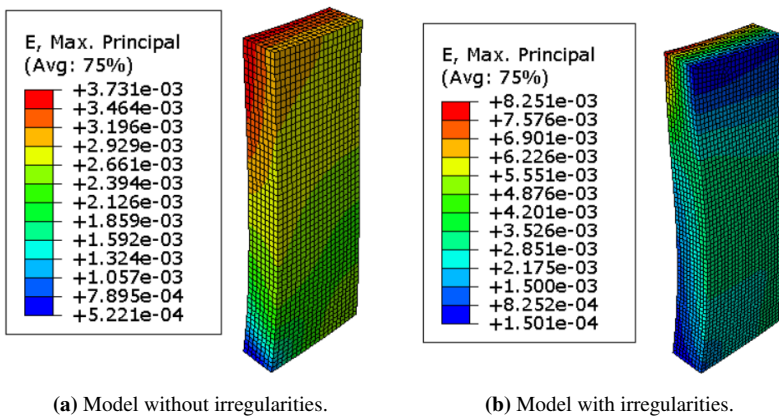
Figure 4.6: The strain distribution on the two specimens.

(a) Model without irregularities.   (b) Model with irregularities.
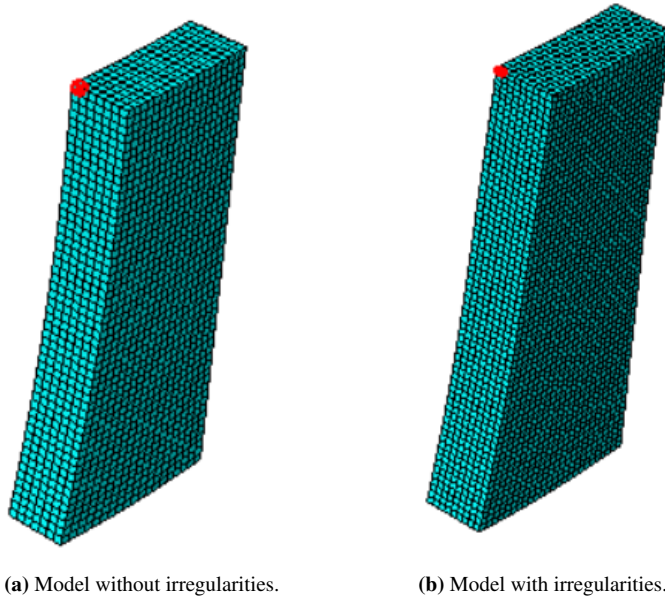
Figure 4.7: The element at the worst point where the strain has been extracted.
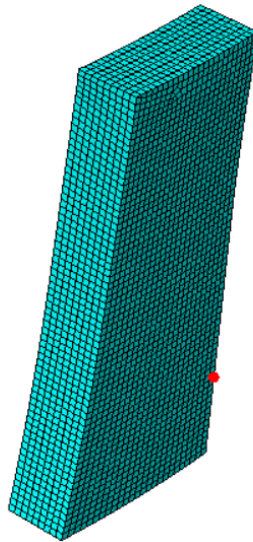
Figure 4.8: The node where the displacement in longitudinal direction was measured for the model with irregularities.

4.3.2 Nominal Strain

To get a good look into which impact the notch had on the strain distribution, the nominal strain for the two cases were compared. To be able to compare the two, the percentage of $\triangle\epsilon$ that replicate the results from the long vectors used on the notched specimen was considered. For **the notched specimen**, the post-processing data was in the desired form, meaning the results could be used directly. For **the smooth specimen**, the percentage of $\triangle\epsilon$ was given in the center, not at the long vector. To obtain the correct values from the finite element model, the same step time as for the equivalent Von Mises strain, where ϵ_{yy} equals ϵ_{abacus} was used. The longitudinal displacement of a node placed on the end of the long vector was then used to find $\triangle\epsilon$, as illustrated in **Fig. 4.9**. In Equation (4.5) the translation from displacement of the node to percentage of $\triangle\epsilon$ is demonstrated.
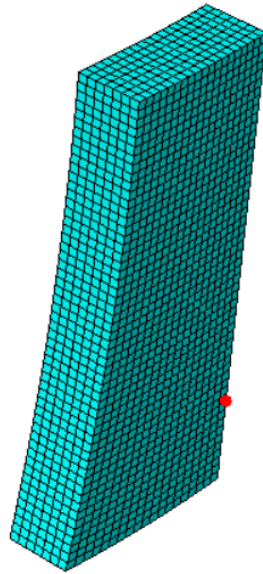
Figure 4.9: The node where the displacement in longitudinal direction of the model without irregularities was measured.

$$\triangle\epsilon = \frac{displacement_{abacus} \cdot 100 \cdot 2}{11mm} \tag{4.5}$$

Chapter 5

Results and Discussion

This chapter contains the main findings of the thesis. The results will be presented and discussed. The goal is to present the result with a discussion to look into the logic behind the findings. First, the results from the two methods explained in Chapter 4 are presented with a brief comment, followed by a discussion.

5.1 Results

The results will be presented separately in this section, following a discussion in the next section. Both graphs and images showing where the failures have occurred will be presented.

5.1.1 Worst Point Equivalent Strain

The results from the fatigue data with strain at the worst point of the specimen are presented as a strain-life curve, with the equivalent strain versus the number of cycles until failure. Factors that might influence the results are the strain rate and the presence of a notch. To evaluate how the strain rate influence the fatigue life, the results for the smooth- and notched specimens must be analyzed. The results for the smooth and notched specimens are presented in **Fig. 5.1** and **Fig. 5.2**, respectively. For both cases, the highest strain rates obtained the highest equivalent strain at the worst point. For the smooth specimens, it seems like the highest strain rate also obtains a somewhat higher number of cycles before failure in general. **Fig. 5.3** illustrates the notched versus the smooth specimen tested at 1E-$2s^{-1}$ and **Fig. 5.4** illustrates the notched versus the smooth specimen tested at 1E-$3s^{-1}$. The equivalent strain at the worst point was much higher for the notched specimens, with an average increase of almost 400% from the smooth specimen.
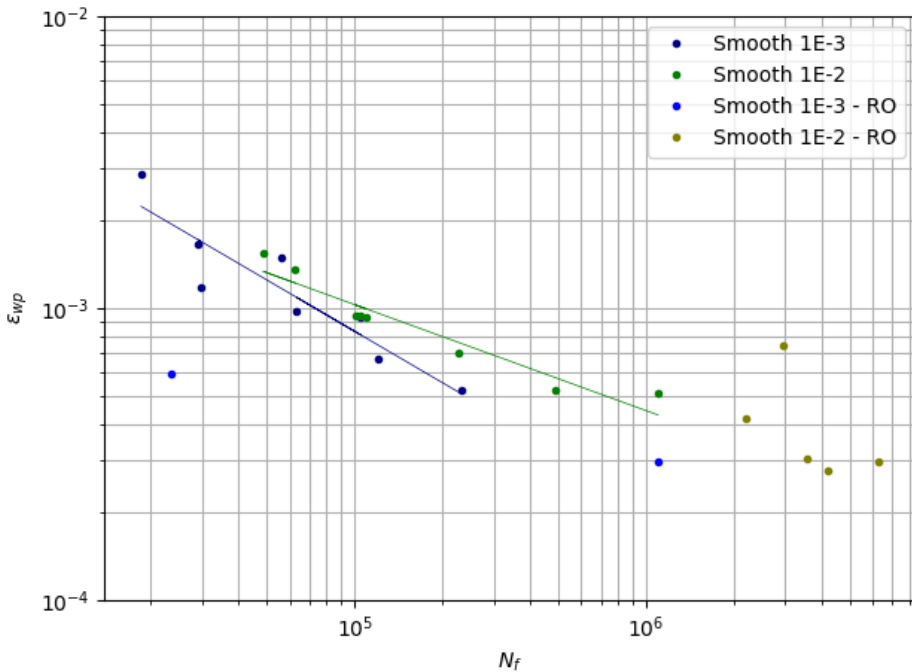
Figure 5.1: Strain-life curve for the smooth specimen at the worst point for $1\text{E-}2s^{-1}$ and $1\text{E-}3s^{-1}$.

5.1.2 Nominal Equivalent Strain

The results from the fatigue data with the nominal strain are presented as a strain-life curve, with the nominal strain in percentage versus the number of cycles until failure. The relevant factors that might influence the results are strain rate and the presence of a notch. To evaluate how the strain rate influence the fatigue life, the results for the smooth- and notched specimens must be analyzed. The results for the smooth and notched specimens are presented in **Fig. 5.5** and **Fig. 5.6**, respectively. For both cases, the highest strain rate obtained the highest nominal strain in general. To analyze how the presence of a notch impact the nominal strain, **Fig. 5.7** shows the results from the notched and the smooth specimen with a strain rate of $1\text{E-}2s^{-1}$. Here one can observe that the smooth specimen obtains a somewhat higher nominal strain and a higher number of cycles before failure. Now, looking at **Fig. 5.8**, which are the results from the notched and the smooth specimen with a strain rate of $1\text{E-}3s^{-1}$, the smooth specimen still obtains a higher nominal strain, but the number of cycles until failure does not vary as much.

5.1.3 Fracture Location

When performing fatigue tests, the location where the fracture occurs is an interesting thing to investigate. When a specimen has a "dog-bone shape" with a thinner middle
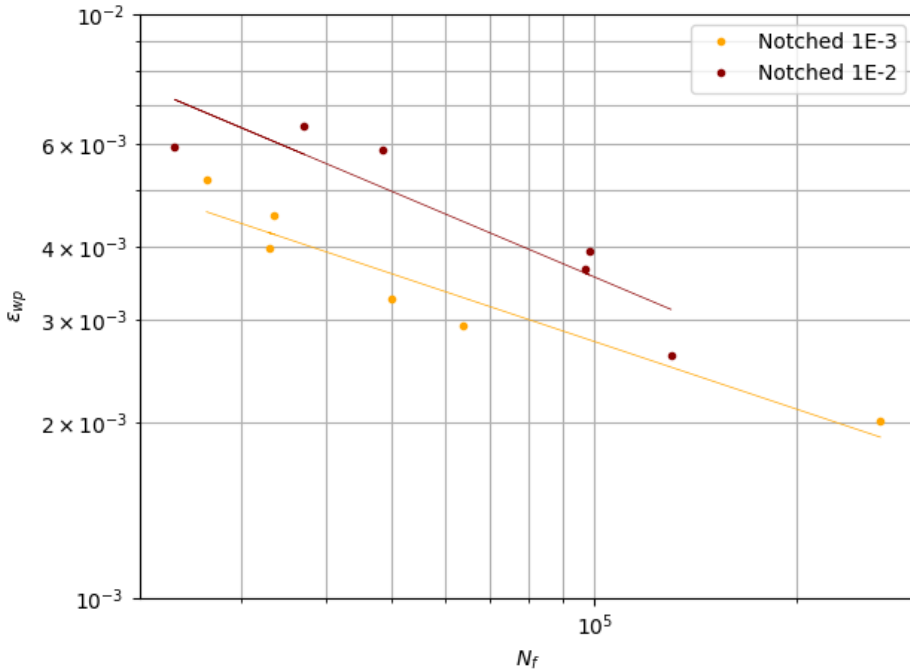
Figure 5.2: Strain-life curve for the notched specimen at the worst point for $1\text{E-}2s^{-1}$ and $1\text{E-}3s^{-1}$.

section, one would expect the fracture to occur in the thinnest section. An example where this occurred on one of the smooth specimens after testing is shown in **Fig. 5.9**. One can observe the fracture going across the middle section, almost normal to the loading direction. If the specimen is subject to cyclic loading and has irregularities, the location of the fracture might differ from the smooth specimen. In **Fig. 5.10** one can observe two of the notched specimens after testing. **Fig. 5.10a** illustrates the fracture propagating from both sides of the specimen normal to the loading direction. For the specimen in **Fig. 5.10b**, the fracture propagates from one side like the for the smooth specimen, with an angle from the loading direction.

5.2   Discussion

The purpose of the discussion is to look into the method and the findings of the thesis, to connect it to existing theory, and look for new links. First, the methodology is discussed, followed by the results and the main findings.
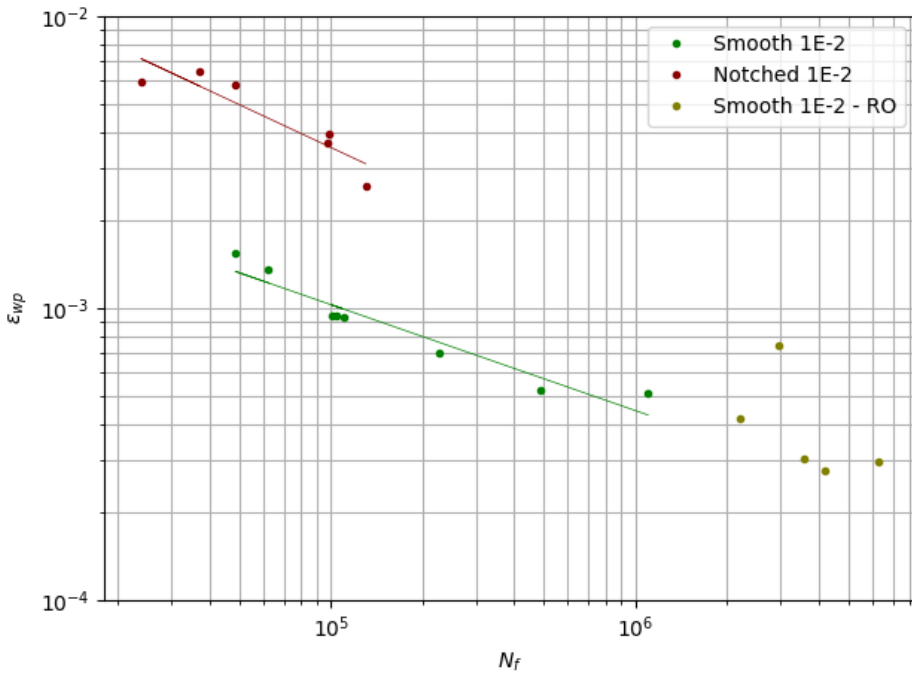
Figure 5.3: Strain-life curve from the worst point for $1\text{E-}2s^{-1}$.

Methodology

The method chosen for material model calibration was to utilize Isight to obtain a material model that fit the experimental data for the three strain rates: $1\text{E-}2s^{-1}$, $1\text{E-}3s^{-1}$, and $1\text{E-}4s^{-1}$. A finite element model was made in Abaqus to replicate the experimental tests. The power law creep model was the creep model that was chosen to recreate the creep behaviour of the material, and the Hooke-Jeeves optimization method was chosen in Isight. Looking at earlier research, like Viespoli et al. (2019c), the authors comment that the power law creep model is desirable for its simplicity at higher strain rates. The Anand creep model could have been applied, but it is more complicated and harder to implement (Viespoli et al., 2019c). Taking that into consideration and looking at the results in **Fig. 3.9**, the chosen creep model is satisfactory for the models in this thesis. As mentioned earlier, Viespoli et al. (2019c) argues that both the strain rate and the thickness of the specimen are significant factors that influence the material response. As this thesis only investigates the thickness of 1.8mm, it should be taken into consideration when applying the results. If a lead sheathing with different thickness is tested, the material model should be properly calibrated again. It is also important to note that the best fit-curves that replicate the experimental results are approximations, which means that the material model is based on approximated data. This means that all the results in this thesis contain uncertainties.
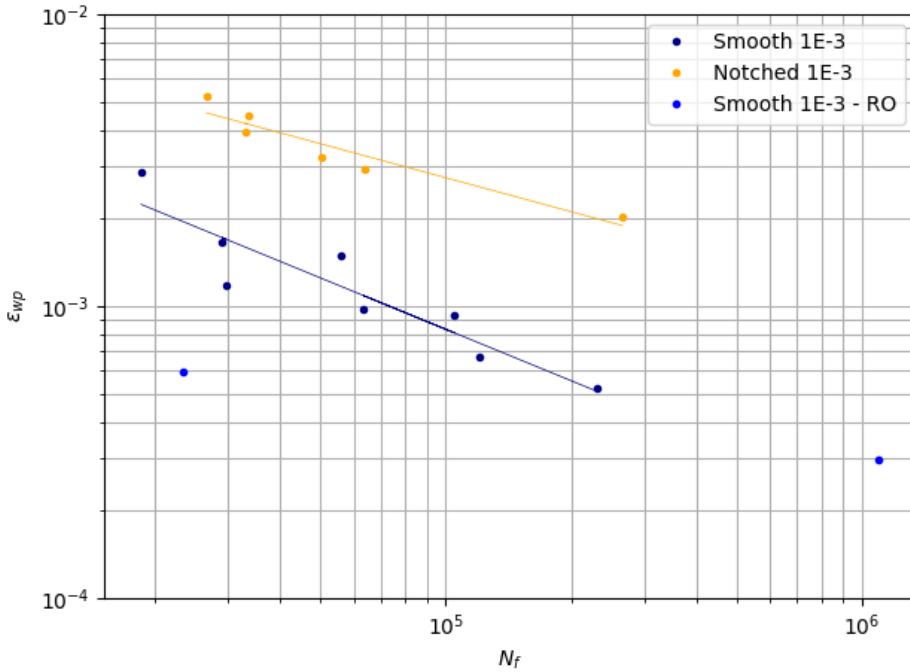
Figure 5.4: Strain-life curve from the worst point for $1\text{E-}3s^{-1}$.

To obtain the required fatigue data, experimental tests were performed by SINTEF, followed by finite element modeling. The experimental testing utilized 2D DIC to obtain the measurements after testing. As mentioned in Section 2.5.2, it is possible to use DIC in both 2D and 3D. According to Pan et al. (2014), 2D DIC is limited to in-plane deformation. As the tests with irregularities already were somewhat out of plane, the results might have been better utilizing 3D DIC. For the finite element modeling of the specimen with irregularity, estimation of the shape and measurements was used. This can result in the finite element analysis giving slightly different results than the experimental testing. The eventual difference in results is acceptable for this thesis due to the goal being to investigate the overall impact of irregularities on fatigue life.

Results and Main Findings

The main goal of this thesis is to look into how irregularities impact the fatigue life of lead sheathings. The first interesting aspect to investigate is how the irregularity changes the strain distribution. **Fig. 4.6** reveals the principal strain distribution for the two models. One can observe that the maximum strain is twice as high for the model with the irregularity. Also, the distribution has changed due to the shape of the irregularity. The point where the highest strain was obtained is the same for the two models, even though the rest
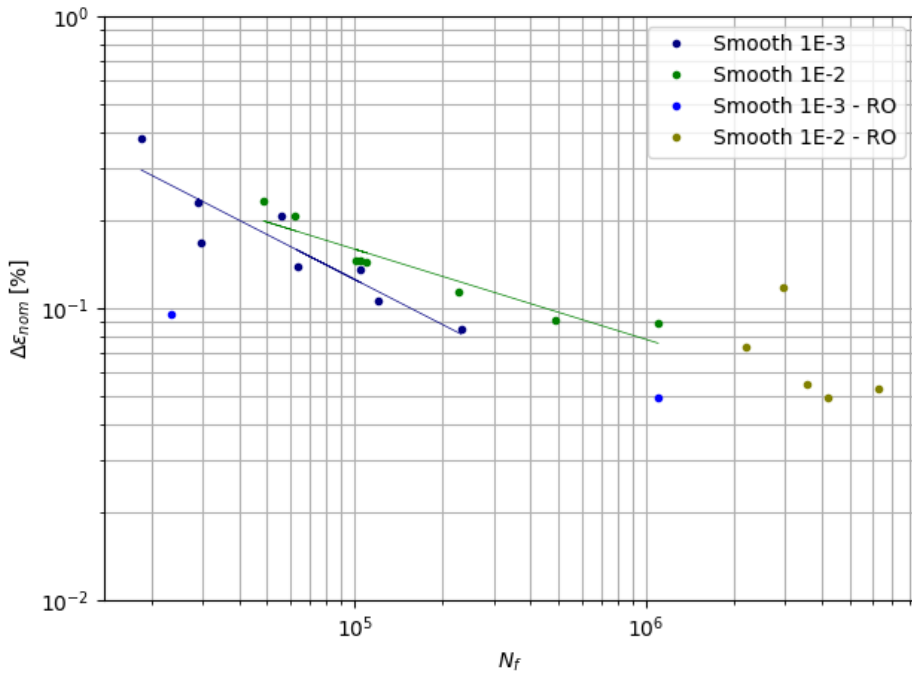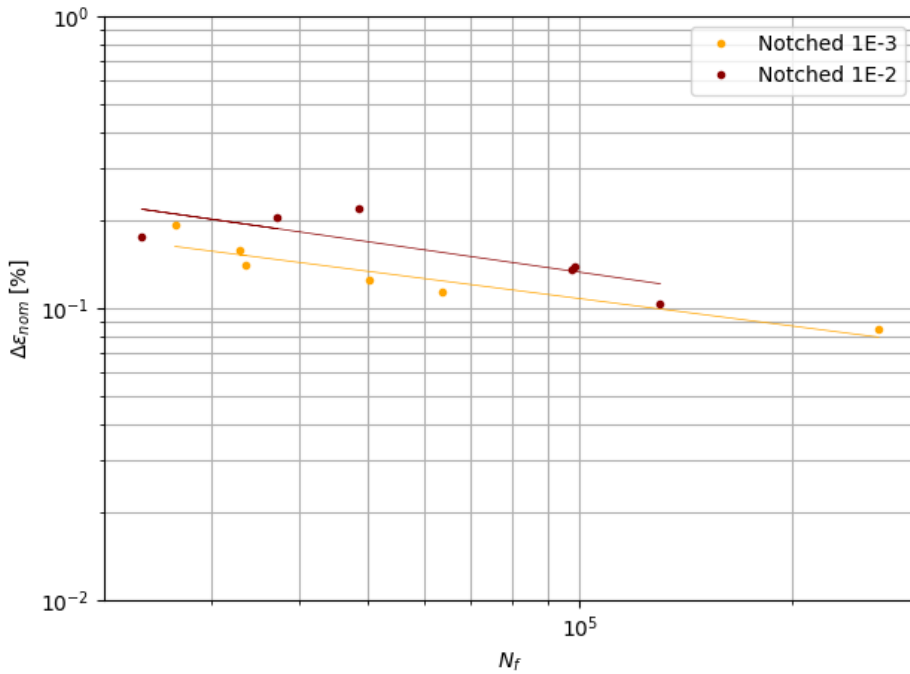
Figure 5.5: Nominal strain-life curve for the smooth specimen 1E-$2s^{-1}$ and 1E-$3s^{-1}$.

seems different. On the model with the irregularity, the "inside" of the blunt notch has a lower strain than the smooth specimen. Looking at these strain distributions makes sense that the nominal strain is higher for the smooth specimen, while the equivalent strain at the worst point is higher for the model with irregularities.

Several aspects need to be addressed, looking at the results from both the equivalent strain at the worst point of the specimen and the nominal strain. The main topics are strain rate dependency, the difference in the nominal- and worst point strain, and the fracture location.

The first thing to evaluate is how the strain rate affects the results. Looking at the results from the experimental cyclic loading in **Fig. 3.3**, one can observe the difference between the three strain rates that were tested. In the article "Tensile characterization of a lead alloy: creep induced strain rate sensitivity", Viespoli et al. (2019c) conclude that the response of the material is highly strain rate sensitive. As creep is present at room temperature, the strain rate becomes important. Looking at **Fig. 2.3 (b)**, the creep curve for constant strain rate reaches a plateau where the material reached the steady state stress, σ_{ss}. Looking at **Fig. 3.3** again, it is apparent that none of the strain rates in this thesis reaches σ_{ss}. Even though none of the tests reached σ_{ss}, the difference is an important factor. As the test at $\dot{\epsilon} = $ 1E-$4s^{-1}$ runs for a much longer time than the test with $\dot{\epsilon} = $ 1E-$2s^{-1}$, there are more creep mechanisms present. In the article "Room temperature creep mech-

Figure 5.6: Nominal strain-life curve for the notched specimen 1E-2s^{-1} and 1E-3s^{-1}.

anisms of a Pb-Sn-Sb lead alloy", Viespoli et al. (2019a) concludes that diffusional creep mechanisms are active in low stress ranges and dislocation creep mechanisms are active in higher stress ranges. In **Fig. 3.3** it is visible that the lower strain rates obtain higher stress levels in these tests. This indicates that the creep mechanisms having the most influence in the tests with different strain rates will vary. In the lower strain rate, where the higher stress levels are reached, are probably dislocation creep of the greatest influence.

Going forward, with the importance of strain rate in mind, the fatigue test results will be investigated deeper. The first thing to consider is the number of cycles until failure for the different strain rates, both with and without irregularities. For the smooth specimens, the number of cycles until failure for tests with $\dot{\epsilon}$ = 1E-3s^{-1} were on average almost 60% lower than for tests with $\dot{\epsilon}$ = 1E-2s^{-1}. For the specimens with irregularities, the number of cycles until failure did not differ with the same majority for the two strain rates. The average difference was only 0.2% due to two of the tests, where the specimens with $\dot{\epsilon}$ = 1E-3s^{-1} had the highest number of cycles. If these two results are taken out of the equation, the specimens tested with $\dot{\epsilon}$ = 1E-3s^{-1} had in average 20% shorter life than for specimens tested with $\dot{\epsilon}$ = 1E-2s^{-1}. Looking at **Fig. 5.11**, the strain rate versus the number of cycles until failure for the specimens are plotted. By looking at these plots, one can see the upward shift in the number of cycles for the tests with a strain rate of 1E-2s^{-1} compared to 1E-3s^{-1} for the smooth specimen. This shift is not as clear for the notched specimens,
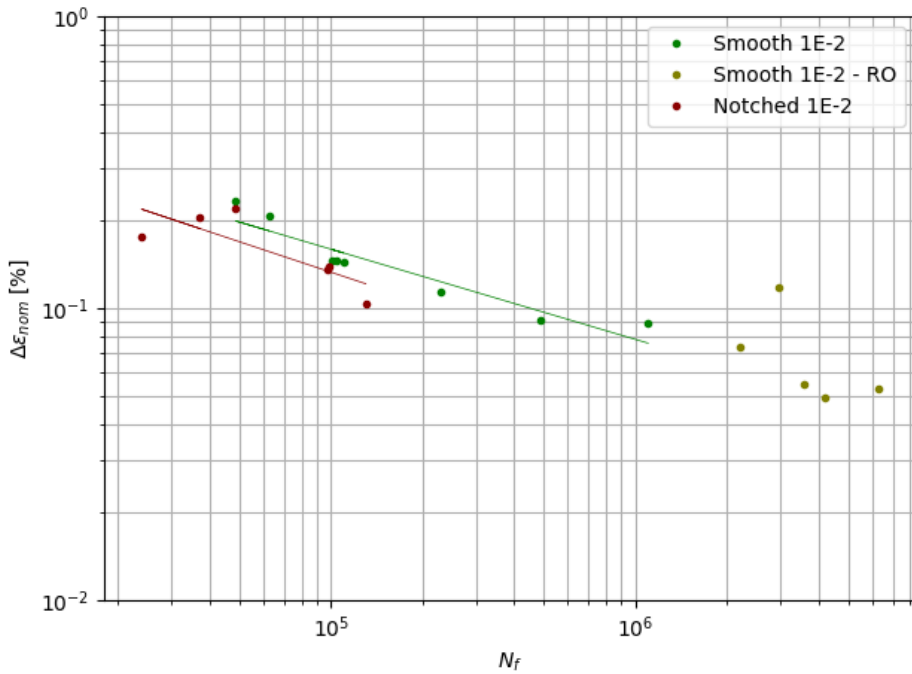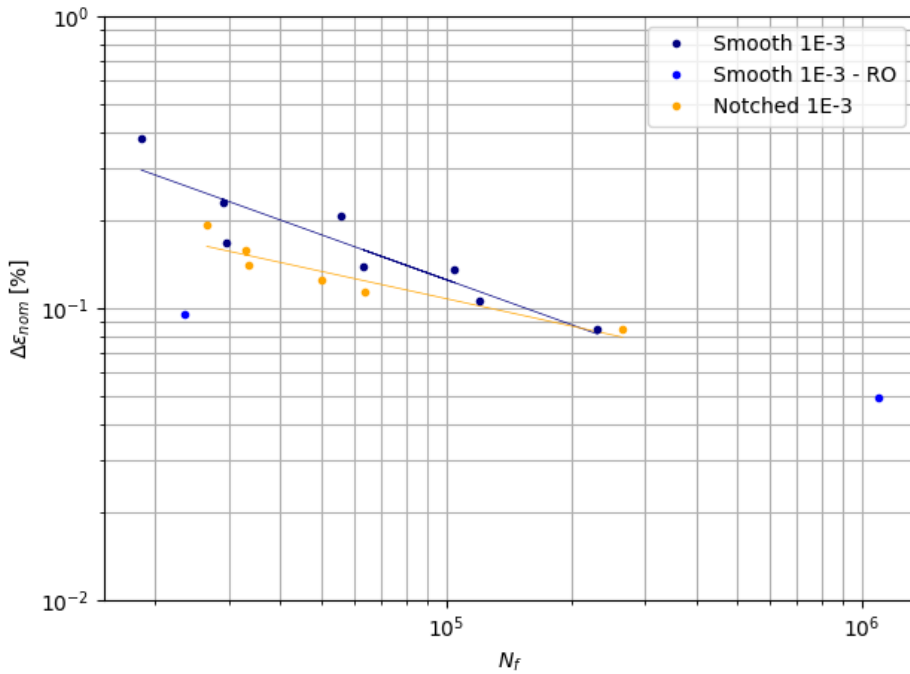
Figure 5.7: Nominal strain-life curve for 1E-2s^{-1}.

due to the difference in the results.

In the article "Small- and Full-Scale Fatigue Testing of Lead Cable Sheathing", Johanson et al. (2019) did multiple fatigue tests with different loading modes and settings. One of the main findings in the article was that the fatigue life of lead strongly depends on the loading mode. In **Fig. 5.12**, the frequency versus number of cycles until failure for the tests with smooth specimens, where the tests with $\dot{\epsilon}$ = 1E-2s^{-1} have ten times the frequency of the tests with $\dot{\epsilon}$ = 1E-3s^{-1}. Looking at **Fig. 5.13**, global strain range versus the number of cycles is plotted. Both the frequency and the strain range are according to Johanson et al. (2019) important factors.

The final thing to discuss considering the results is the notch impact on fatigue life. The reduction in fatigue life because of the notch was different for the two strain rates. For the tests with a strain rate of 1E-2s^{-1}, the notched specimen had, in average 70% shorter life than the smooth specimen. For the tests with a strain rate of 1E-3s^{-1}, the average decrease in fatigue life was 30%. Earlier research by Johanson et al. (2018) and Viespoli et al. (2019b) both investigate how a notch impact fatigue life and the material. The notch in this thesis is blunter than from the articles where the notch is made as a blind hole on the convex side of the specimen, and the results might differ accordingly. Considering the results from the equivalent strain at the worst point of the models, it is clear that the

Figure 5.8: Nominal strain-life curve for 1E-3s^{-1}.

notched specimens obtained a higher equivalent strain. For the tests with the strain rate of 1E-2s^{-1} the average increase of equivalent strain at the worst point for the notched specimen was 450%. For the tests with the strain rate of 1E-3s^{-1} the average increase of equivalent strain at the worst point for the notched specimen was 385%. Looking at the results from the nominal strain, the smooth specimens obtained a somewhat higher strain.

In the article "Strain controlled medium cycle fatigue of a notched Pb-Sn-Cd lead alloy", Viespoli et al. (2019b) argue that because of the material having a highly plastic behaviour, the notch sensitivity is minimal. As explained in Section 2.4.1, the notch sensitivity is a measure of how a specimen is affected by a notch. Because lead is a ductile material, it is expected that the notch sensitivity is low, meaning it often has a high tolerance to a local increase of stress and strain. Looking at how the equivalent strain at the worst point of the specimen is higher for the notched specimen, but the nominal strain range is higher for the smooth specimen, it seems like the notch sensitivity, q, is low. In the article "Experimental and numerical investigation of strain distribution of notched lead fatigue test specimen" by Johanson et al. (2018), the authors argue that the notch effect is different for different strain ranges and dependent on the frequency. In the article, the strain ranges are 0.15% and 0.28%, and the results indicate that the notch impact is almost zero for the highest strain range. Looking at the results presented in this thesis, one can observe that the difference in N_f is more significant for the lower strain ranges. This indicates that the notch
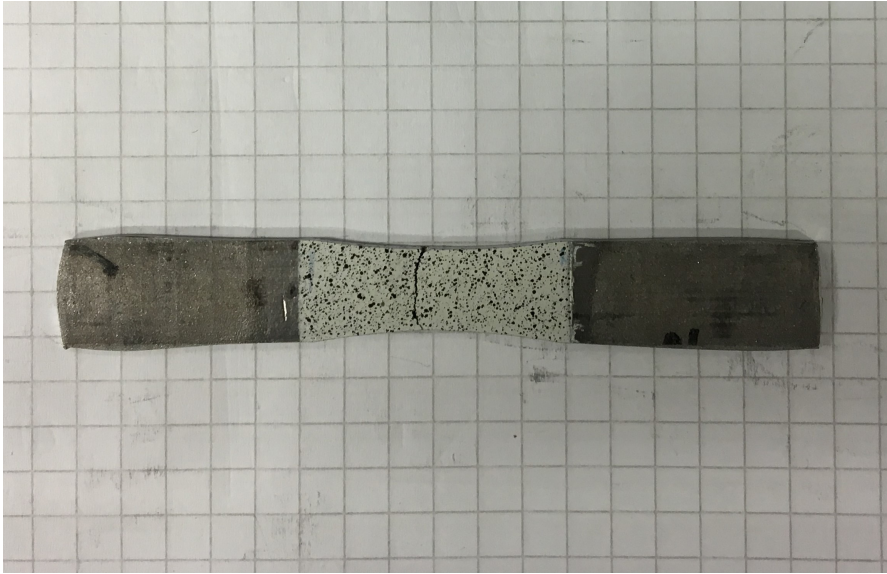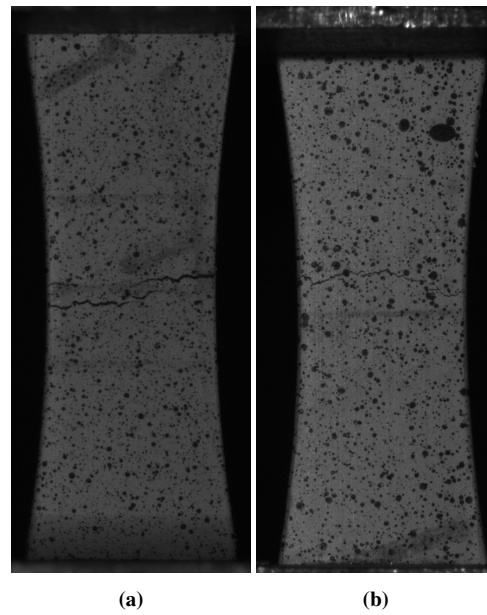
**Figure 5.9:** An example of the location of a fracture on a smooth specimen.

impact is higher for lower strain ranges.

Another aspect of how irregularities can impact fatigue life is the location and propagation of the cracks. **Fig. 5.9** and **Fig. 5.10** demonstrates one example of a smooth specimen and two examples of specimens with irregularities after failure. It does not seem to be a huge difference in how the crack propagates. Viespoli et al. (2019b) argue that the propagation of fatigue cracks often happens at $45°$ of the loading direction, and therefore is strongly influenced by mode II fracture propagation. Looking at the results here, in particular **Fig. 5.10b**, it looks like the crack propagation is at $45°$ of the loading direction. These results indicate that it is a mixed-mode fracture and that it is difficult to know the propagation path of the cracks in advance. As these tests have blunt notches over the whole specimen's width, it is harder to see how the crack starts and propagates. As Johanson et al. (2018) mentions, it has to be kept in mind that lead sheathings are tubular, which means the cracks starting at the edge of test specimens are test artifacts. Thus, the testing of the specimens in this thesis is conservative compared to the real-life components.

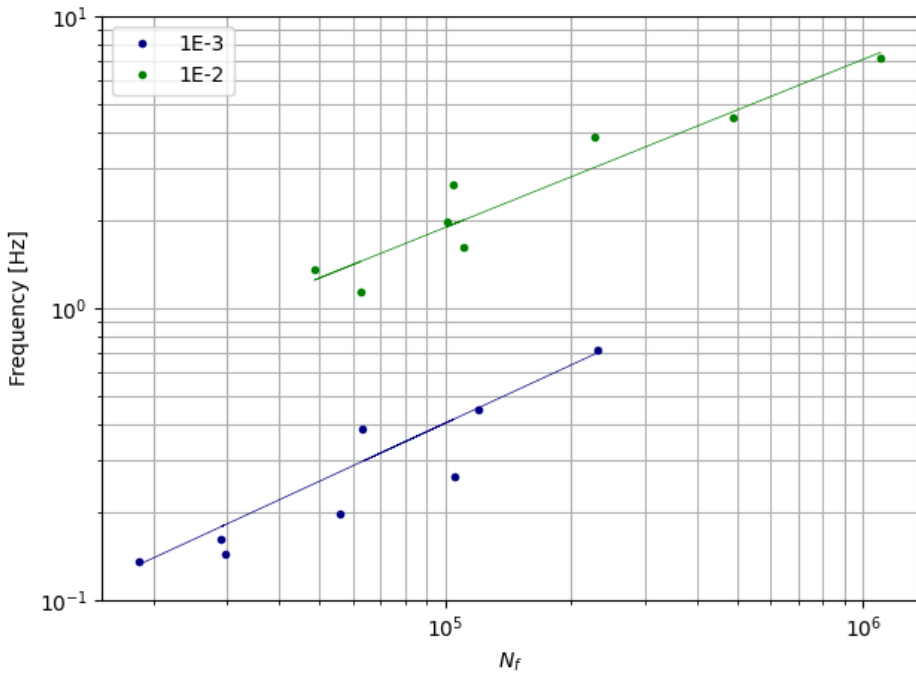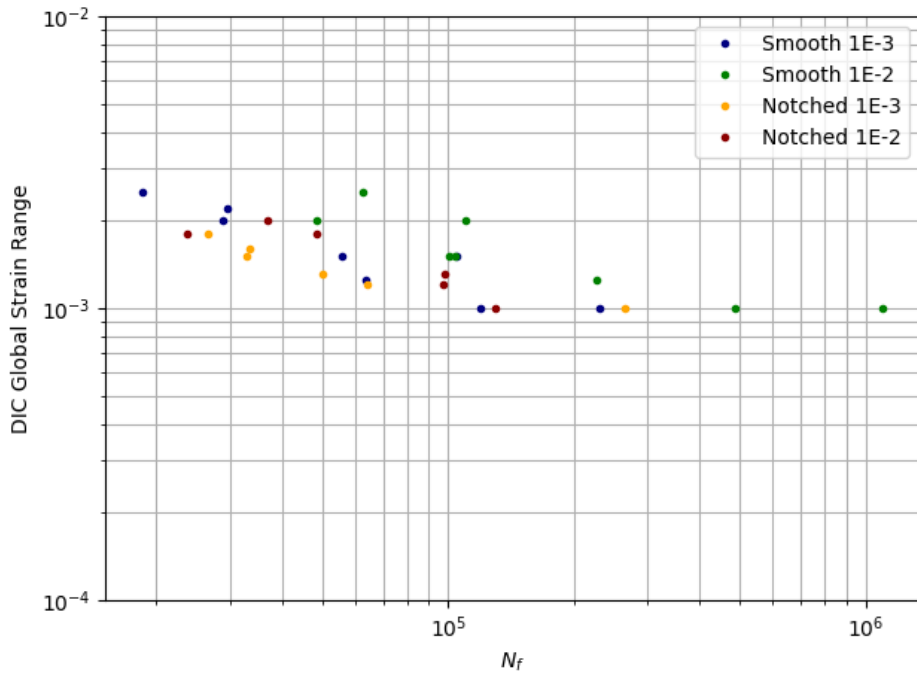(a)   (b)

Figure 5.10: Two examples of the location of a fracture on two notched specimens.
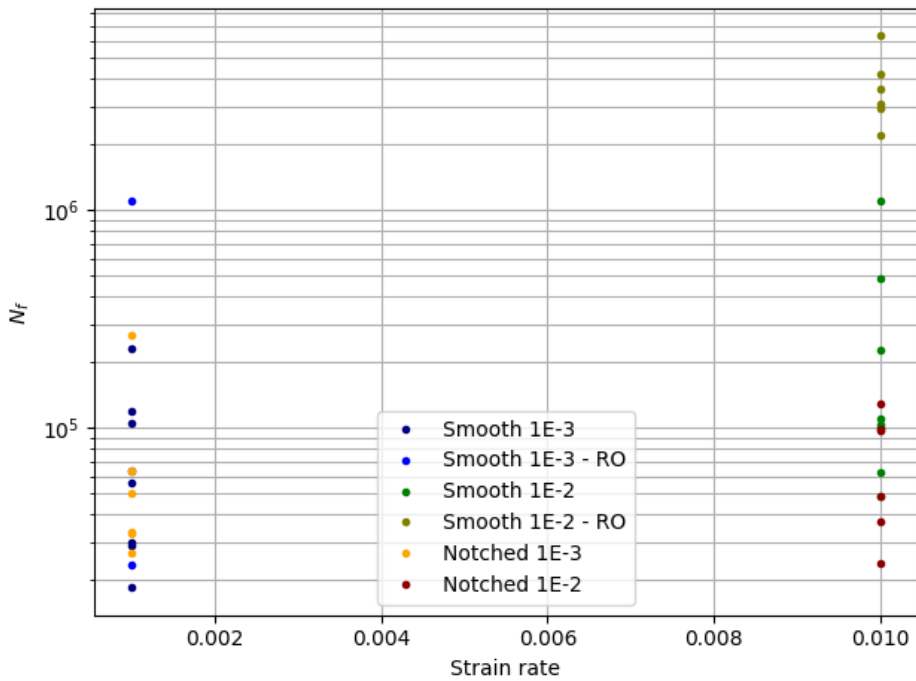
Figure 5.11: Strain rate versus number of cycles until failure for fatigue testing.

Figure 5.12: Frequency versus the number of cycles until failure for the fatigue testing.

Figure 5.13: The global strain range versus number of cycles until failure for fatigue testing.

Chapter 6

Conclusion

This chapter contains the final conclusions of the thesis, followed by a recommendation for further work.

Conclusion

The purpose of this master thesis has been to investigate how irregularities impact the fatigue life of lead sheathings for underwater cables. To interpret the material response to cyclic loading, a deep understanding of the physics is necessary. Results from experimental testing have been used to generate a calibrated material model that replicates the material behaviour during cyclic loading. The material model was calibrated in Isight, using Hooke-Jeeves as the optimization method, and the creep model applied is power law creep. The material model was then implemented in finite element models, with and without irregularities, subject to cyclic loading. The material tested is a lead alloy E, which is a ductile material sensitive to strain rate, and the fatigue tests have been conducted with two different strain rates: 1E-2s^{-1} and 1E-3s^{-1}.

Finite element models have been developed for both the smooth specimen and the specimen with irregularities. These models simulated physical fatigue testing by conducting tests with cyclic loading in Abaqus. Results from experimental fatigue testing have been used to extract the corresponding data from the finite element analysis for the smooth and notched model. To present the results clearly, they have been presented in strain-life curves. The nominal strain and the equivalent strain in the worst point of the specimens have been considered. From the results, one can observe that the models with irregularities obtain the highest equivalent strain, while the curves for nominal strain-life are higher for the smooth specimens. The results do not show any specific differences in how the cracks propagated in the smooth and the notched test specimens.

For testing at a strain rate of 1E-2s^{-1}, the average reduction in life was 70%, and for testing at a strain rate of 1E-3s^{-1}, the average reduction was 30%. Because of this, the conclusion is that the impact of irregularities shortens the fatigue life. A test artifact is that

most cracks did initiate on the sides of the test specimens. In real life, the lead sheathings are tubular, and they will not obtain the stress concentration observed in the test specimens. The results indicate that the notch sensitivity is low in the lead sheathings. This thesis is limited to the two strain rates, and strain ranges between 0.1% and 0.25%, which should be taken into account for future research.

Further Work

This study has been performed over a short period and with limited resources. Therefore there are some recommended measures to be addressed in the future. To get a deeper understanding and more tangible results, it is necessary to do more research. The first thing that should be done is to get real measurements of the test specimens, to ensure that the finite element models match the experimental test specimens. The correct measurements will ensure that the solutions are comparable to each other. It is advised to compare the strain distribution from the finite element analysis and DIC, both with and without irregularities. First, this will ensure that the FEM can replicate the real results. Secondly, it will give a better indication of where the crack initiation should be and if there are differences between the smooth and the notched model. The crack propagation should be looked more in-depth into and how irregularities change the propagation.

Another aspect that should be considered in further work is to perform more tests with the same loading modes. More tests with comparable data are needed to better understand the fundamental factors that influence the fatigue life. There could, for instance, be multiple tests with the same strain range, with different strain rates or frequencies. This would probably give a better understanding of why the results might differ from one test to another. It is recommended to perform several tests with the same loading modes, to ensure that the results do not contain errors due to test errors.

It is recommended to conduct tests that induce creep, to evaluate how creep influences the lead sheathings. This can be done by decreasing the strain rate or increasing the temperature closer to the melting temperature. Inducing creep would give a deeper understanding of how the material behaves. Lastly, it is recommended to investigate how the thickness of the sheathing affects the fatigue life, with and without irregularities. This would require new material models and in-depth investigation because of the possible change in microstructure for the different thicknesses. It would be smart to optimize the thickness on the sheathing to withstand the cyclic loading, both with and without irregularities, to make it as cost-effective and resistant to failure as possible.

Bibliography

Anelli, P., Donazzi, F., Lawson, W., 1988. The fatigue life of lead alloy e as a sheathing material for submarine power cables. IEEE Transactions on power delivery 3, 69–75.

Bhaduri, A., 2018. Mechanical Properties and Working of Metals and Alloys. Springer.

Campbell, A., Tsao, S., Turnbull, D., 1987. The effect of au and ag additions on the power-law creep behavior of pb. Acta Metallurgica 35, 2453–2464.

Casas, J.S., Sordo, J., 2011. Lead: chemistry, analytical aspects, environmental impact and health effects. Elsevier.

Dassault Systems, 2017. SIMULIA User Assistance 2017.

DIANA, 2012. 32.1.1 equivalent von mises strain. URL: `https://dianafea.com/manuals/d944/Analys/node405.html`.

Dowling, N.E., 2012. Mechanical behavior of materials: engineering methods for deformation, fracture, and fatigue. Pearson.

Fagerholt, E., 2017. ecorr v4.0 documentation — ecorr digital image correlation 4.0 documentation. URL: `http://folk.ntnu.no/egilf/ecorr/doc/index.html`.

Guruswamy, S., 1999. Engineering properties and applications of lead alloys. CRC Press.

Havard, D., 1972. Fatigue of lead cable-sheathing alloys. 24, 11–18.

Hofgaard, M.E., 2018. Defining Local Stress-Strain Fields in Ductile Components under Cyclic Loading. Master's thesis. NTNU.

Holdsworth, S., 2015. Creep-fatigue failure diagnosis. Materials 8, 7757–7769.

Hosford, W.F., 2010. Mechanical behavior of materials. Cambridge university press.

Johanson, A., Viespoli, L.M., Alvaro, A., Berto, F., 2019. Small and full-scale fatigue testing of lead cable sheathing .

Johanson, A., Viespoli, L.M., Nyhus, B., Alvaro, A., Berto, F., 2018. Experimental and numerical investigation of strain distribution of notched lead fatigue test specimen .

Kammer, D., 2014. Slip Fronts at Frictional Interfaces: A Numerical and Theoretical Study. Ph.D. thesis. doi:`10.5075/epfl-thesis-6492`.

Kassner, M.E., 2015. Fundamentals of creep in metals and alloys. Butterworth-Heinemann.

Langdon, T.G., Mohamed, F.A., 1978. A simple method of constructing an ashby-type deformation mechanism map. Journal of Materials Science 13, 1282–1290.

McCormick, N., Lord, J., 2010. Digital image correlation. Materials today 13, 52–54.

McKeen, L.W., 2016. Fatigue and tribological properties of plastics and elastomers. William Andrew.

Mohamed, F., Murty, K., Morris, J., 1973. Harper-dorn creep in al, pb, and sn. Metallurgical Transactions 4, 935–940.

Monfared, V., 2018. Review on creep analysis and solved problems, in: Tanski, T., Sroka, M., Zielinski, A. (Eds.), Creep. IntechOpen, Rijeka. chapter 10. URL: `https://doi.org/10.5772/intechopen.71184`, doi:`10.5772/intechopen.71184`.

Nexans, 2019. Global ekspert på kabler og kabelsystemer. URL: `https://www.nexans.no/eservice/Norway-no_NO/navigate_-22/Global_expert_in_cables_and_cabling_systems.html`.

Pan, B., Yu, L., Wu, D., 2014. Accurate ex situ deformation measurement using an ultra-stable two-dimensional digital image correlation system. Applied optics 53, 4216–4227.

Pelleg, J., 2014. Time-dependent deformation: Creep, in: Mechanical Properties of Ceramics. Springer, pp. 417–530.

Raj, R., Ashby, M., 1971. On grain boundary sliding and diffusional creep. Metallurgical transactions 2, 1113–1127.

Schreier, H., Orteu, J.J., Sutton, M.A., et al., 2009. Image correlation for shape, motion and deformation measurements: Basic concepts, theory and applications. volume 1. Springer.

Sommacal, A., 2018. EXPERIMENTAL AND NUMERICAL INVESTIGATIONS OF A LEAD ALLOY USED IN SUBSEA POWER CABLE. Master's thesis. NTNU.

Thornton, I., Rautiu, R., Brush, S., 2001. Lead the facts. IC Consultants Ltd, London, UK .

Viespoli, L.M., Johanson, A., Alvaro, A., Nyhus, B., Berto, F., 2019a. Room temperature creep mechanism of a pb-sn-sb lead alloy. Procedia Structural Integrity 18, 86–92.

Viespoli, L.M., Johanson, A., Alvaro, A., Nyhus, B., Berto, F., 2019b. Strain controlled medium cycle fatigue of a notched pb-sn-cd lead alloy. Engineering Failure Analysis 104, 96–104.

Viespoli, L.M., Johanson, A., Alvaro, A., Nyhus, B., Sommacal, A., Berto, F., 2019c. Tensile characterization of a lead alloy: creep induced strain rate sensitivity. Materials Science and Engineering: A 744, 365–375.

Zhang, J.S., 2010. High temperature deformation and fracture of materials. Elsevier.

Appendix

Appendix A

Best Fit Curves - Experimental Results

$\sigma[MPa]$	ϵ
0	0
4	0.000268733
4.5	0.00030471
5	0.000343173
5.5	0.000385829
6	0.000435213
6.5	0.000494963
7	0.000570147
7.5	0.000667645
8	0.0007966
8.5	0.000968934
9	0.001199938
9.5	0.001508941
10	0.001920063
10.5	0.002463053
11	0.003174221

Table A.1: Best fit curve for 1E-2s^{-1}

$\sigma[MPa]$	ϵ
0	0
4	0.000270966
4.5	0.000309688
5	0.000353368
5.5	0.000405326
6	0.000470447
6.5	0.000555682
7	0.000670636
7.5	0.000828252
8	0.001045615
8.5	0.00134486
9	0.001754209
9.5	0.002309137
10	0.003053673

Table A.2: Best fit curve for 1E-3s^{-1}

$\sigma[MPa]$	ϵ
0	0
4	0.000285895
4.5	0.00033926
5	0.000407681
5.5	0.00049914
6	0.000624467
6.5	0.000797945
7	0.001038
7.5	0.001367931
8	0.001816716
8.5	0.00241988
9	0.003220422

Table A.3: Best fit curve for 1E-4s^{-1}

Appendix B

FEM without Irregularities
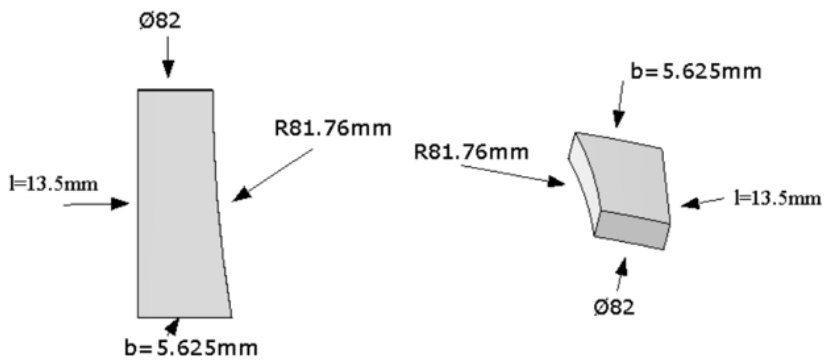
Figure B.1: FEM dimensions of the model without irregularities.

Appendix C

Plastic Properties

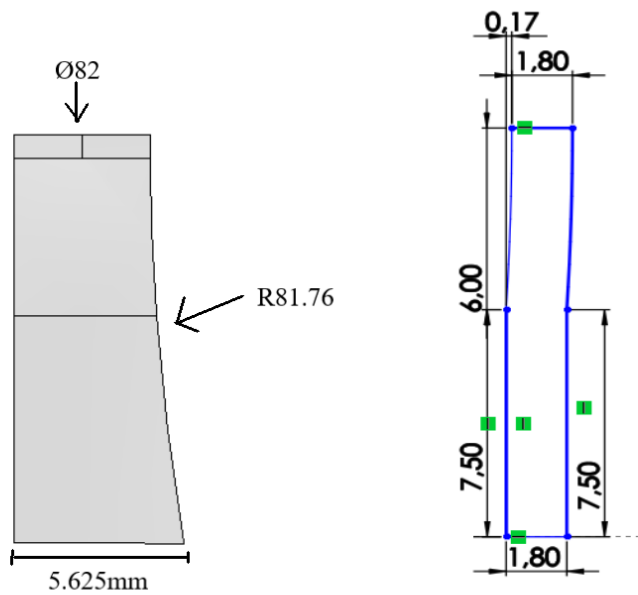| $\sigma[MPa]$	ϵ_{pl}
7	0
7.5	0.000121457
8	0.000186758
8.5	0.000279773
9	0.00040954
9.5	0.000587269
10	0.000826698
10.5	0.001144481
11	0.001560623
11.5	0.002098935
12	0.002787544
12.5	0.00365943
13	0.004753013
13.5	0.006112776
14	0.007789931
14.5	0.009843133
20	1

Table C.1: Plastic properties for the finite element models in Abaqus.

Appendix D

FEM with Irregularities

Figure D.1: FEM dimensions of the model with irregularities.